Dissertations, Theses, and Masters Projects   Theses, Dissertations, & Master Projects

1993

Boundary Layer Structure in Homogeneous Tidal Flows: A Theoretical and Numerical Study

Jian Shen

College of William and Mary - Virginia Institute of Marine Science

Recommended Citation

BOUNDARY LAYER STRUCTURE IN HOMOGENEOUS TIDAL FLOWS:

A THEORETICAL AND NUMERICAL STUDY

A Thesis

Presented to

The Faculty of the School of Marine Science

The College of William and Mary

In Partial Fulfillment
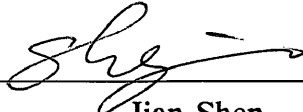
Of the Requirements for the Degree of

Master of Arts

----

by
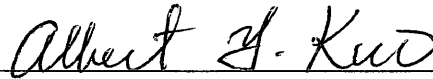
Jian Shen

1993

This thesis is submitted in fulfillment of
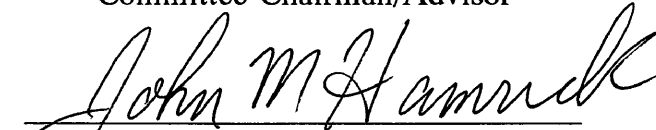
the requirements of the degree of

Master of Arts

_____
Jian Shen

Approved, July 1993

_____
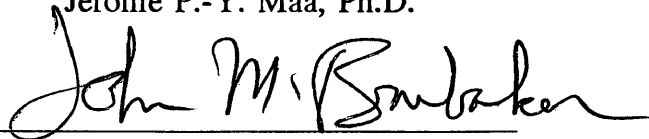Albert Y. Kuo, Ph.D.
Committee Chairman/Advisor
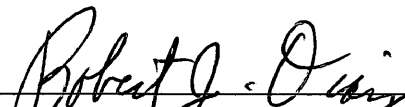
_____
John M. Hamrick, Ph.D.
Co-chairman

_____
Jerome P.-Y. Maa, Ph.D.

_____
John M. Brubaker, Ph.D.

_____
Robert J. Diaz, Ph.D.

TABLE OF CONTENTS

ACKNOWLEDGEMENTS

LIST OF FIGURES

ABSTRACT

A theoretical analysis of the boundary layer flow is performed to derive a formulation specifying the bottom shear stress boundary condition in an unsteady, homogeneous tidal flow model. The unsteady boundary layer equation is solved for the velocity distribution adjacent to the boundary using a regular perturbation expansion. When applied to the bottom layer of the computation grid of a numerical model, the solution relates the bottom shear stress to the velocity and acceleration computed in that layer. The zero order solution of near bottom velocity profile consists of two parts, one is equivalent to the logarithmic profile and the other is the correction for non-constant stress effect. The first order solution of velocity profile is the contribution of inertial effect. The formulation of bottom tress was obtained by solving the velocity profile which consists two terms, the first term incorporates the correction of non-constant stress effect into the drag coefficient and the second term is the first order correction for inertial effect due to flow unsteadiness.

Numerical experiments with a hypothetical homogeneous estuary indicate that the first order correction term could have a significant effect on calculated bottom stress while having little effect on the velocity. The error in calculated bottom stress increases with vertical grid spacing if the logarithmic profile is used to relate bottom stress to velocity. The inclusion of the correction of both inertial and non-constant stress effect can significantly reduce this error. For a practical range of vertical grid spacing in numerical models of estuarine flow, the new formulation obtained from present study can adequately specify the boundary condition. The numerical experiments also show that, if the roughness height and bottom stress are estimated by fitting a logarithmic profile to the velocity distribution, they may be off by more than 100% if dada used for regression are outside of the logarithmic layer or data obtained are around the phase of high flow acceleration.

BOUNDARY LAYER STRUCTURE IN HOMOGENEOUS TIDAL FLOWS:

A THEORETICAL AND NUMERICAL STUDY

1. INTRODUCTION

1.1 Problem Description

The logarithmic velocity profile has been widely used to calculate the boundary shear stress, drag coefficients, and eddy diffusivities for a large class of oceanic, estuarine and river flows. The flow conditions leading to the logarithmic profile assume steady, uniform, and unstratified flow in a constant stress layer adjacent to a wall boundary. Under these conditions, the velocity gradient at a height z, much greater than the hydraulic roughness height z_0 but much less than the boundary layer thickness δ, is a function of z and the friction velocity u_* only. Dimensionally this gives

$$\frac{du}{dz} = \frac{u_*}{\kappa z} \tag{1.1.1}$$

where u is the mean velocity and κ is von Karman's constant. This integrates to give the familiar logarithmic profile

$$u = \frac{u_*}{\kappa} \ln(\frac{z}{z_0}) \tag{1.1.2}$$

From equation (1.1.1), the kinematic eddy viscosity at elevation z is related to u_* by

$$A_v = \kappa u_* z$$

It has been a common practice to obtain the bottom (kinematic) shear stress, $\tau_b = u_*^2$

and z_0 by fitting equation (1.1.2) to the velocity data measured at some heights above the bottom, or to estimate shear stress from the flow velocity u(z) at a single fixed elevation z above the bed by

$$\tau_b = C_D(z) u^2(z) \tag{1.1.3}$$

where the friction coefficient

$$C_D = \frac{\kappa^2}{\ln^2\left(\dfrac{z}{z_0}\right)} \tag{1.1.4}$$

(e.g. Stermberg, 1972; Wright,1989). The reference elevation z at which u(z) is measured is conventionally 1 m, and the corresponding friction coefficient is referred as C_{100}. In numerical models of estuarine flow, the same formula is often used to specify the bottom boundary stress i.e.

$$\tau_b = C_D |u_1| u_1 \tag{1.1.5}$$

where u_1 is the velocity at height $\Delta z/2$, and Δz is the thickness of the bottom layer. The friction coefficient C_D is given by

$$C_D = \frac{\kappa^2}{\ln^2\left(\dfrac{\Delta z}{2 z_0}\right)} \tag{1.1.6}$$

(e.g., Blumberg and Mellor,1987; Hamrick, 1992).

The field data that have been acquired over the past few years show that boundary layer quantities such as τ_b, z_0 and C_D are appreciably affected by such naturally occurring phenomena as: (1) acceleration and deceleration of tidal flows, (2) wave-current interactions, (3) bed roughness, (4) sediment transport, and (5)

stratification (Wright, 1989). Because of the complicacy of the nature of estuarine flow, caution must be exercised when treating the boundary layers associated with these flows. Some of the assumptions used to derive equation (1.1.2) may not be satisfied so that equations (1.1.3)-(1.1.6) might not be applicable to calculate the bottom shear stress.

Tidal currents near the floor of estuaries are not steady. During the accelerating or decelerating phases of tidal flows, velocity often departs from a logarithmic profile. There are prototype data (Soulsby and Dyer, 1981; Gross and Nowell, 1983) demonstrating deviation from equation (1.1.2), and on the other hand, there are also data supporting its acceptability for estuarine flows (e.g., Anwar, 1981, 1983; Wilkinson, 1986). Apparently, the degree of deviation from the logarithmic velocity profile due to acceleration and deceleration depends on some dynamic parameters of estuarine boundary layer flow. More quantitative investigations of the boundary layer structure in oscillatory flows are warranted and more complicated models are usually invoked.

For a depth limited oscillatory flow, the thickness of the constant stress layer is much thinner than that in a steady flow (Dyer 1986). Thus the application of equations (1.1.3) and (1.1.4) are further restricted. In the outer layer (above the constant stress layer), flow is highly affected by external conditions. It is also determined by the wall shear stress far upstream, if the flow has a reasonable long memory (Dyer 1986). As the shear stress and turbulence energy diminishes towards the surface, the velocity profile departs from the logarithmic profile significantly. There are prototype data showing that the velocity above the constant stress layer is larger than that estimated by the logarithmic profile. (Gross and Nowell 1983, Dyer 1986). Consequently, the bottom shear stress will be overestimated when using equations (1.1.3) and (1.1.4) in

the outer layer. For a numerical model of tidal flow with large grid spacing, error may also be introduced when equations (1.1.5) and (1.1.6) are used to specify the bottom boundary condition. Because of the effect of non-constant stress in the outer layer, it is more difficult to relate bottom stress to the flow away from the bottom. The relationship between bottom stress and the flow well above the bottom need to be resolved.

The interaction of the flow acceleration and deceleration, the effects of stratification, sediment re-suspension and deposition in estuaries results in more difficulty in studying estuarine flow structure. Many field measurements and laboratory experiments have been reported and significant advances have been made in recent years, but because of the difficulty in isolating the essential feature of time-dependent boundary layer flows in the field, few experiments and measurements have been conducted in unsteady estuarine flow either stratified or well-mixed. Results reported by different authors are conflicting. Many features of flow structure in estuarine oscillatory turbulent boundary layer, and its effects on turbulence and its related parameters still need to be resolved. First, the effect of acceleration on velocity profile near the bottom needs to be quantified, in particular, what deviations from the logarithmic velocity profile are caused by accelerating flow, and over what part of the tidal cycle. Second, the effect of non-constant stress on the velocity profile needs to be determined. Third, the relationship between flow structure and shear velocity or bottom shear stress needs to be ascertained, as well as the bulk relationship between bottom shear stress and flow well above the bottom in estuaries.

value of u_* was compared with Reynolds stress obtained from the field measurements. They found that when flows are accelerating or decelerating, $<u'w'>^{1/2}<0.7u_{**}$. The boundary shear stress, ρu_*^2 and Reynolds stress $-<\rho u'w'>$ were found to agree to within 40%. The closest agreement occurred at maximum flow when there was no acceleration.

Soulsby and Dyer (1981) indicated that a logarithmic velocity profile is no longer valid under accelerating flow unless a correction term proportional to $z-z_0$ is added. Using similarity and dimensional argument, they derived a log-linear expression for near-bed velocity profile in an unsteady tidal flow.

$$u=\frac{u_*}{k}[\ln(\frac{z}{z_0})-\frac{z-z_0}{\gamma L_a}]$$

(1.2.1)

where L_a is an acceleration length scale defined as

$$L_a=\frac{u_*|u_*|}{\partial_t u_*}$$

and 'γ' is a proportionality constant depending on bed roughness and $\partial_t u_*$ is the time derivative of shear velocity. They pointed out that, by fitting a logarithmic velocity profile, u_* and z_0 may be underestimated by as much as 20% and 60% in an accelerating flow and as much as 20% and 83% in a decelerating flow, respectively. They suggested a criterion for unsteady effects to be negligible as $|z/L_a|<0.005$. The velocity profiles measured near the bed in tidal flows in Start Bay and Weymouth Bay agreed reasonably well with the theoretical formula (equation 1.2.1).

Lavell and Mofjeld (1983) introduced a more complicated semi-analytic model of a time-dependent bottom boundary layer to study the effects of acceleration on flow profiles. The departures of the velocity profile from the logarithmic profile were also observed. This model indicates that fitting a logarithmic profile would result in an underestimate of u_* during most of the accelerating cycle and part of the decelerating cycle. The corresponding underestimate of maximum bottom shear stress can be up to 60%.

On the other hand, some field measurements and laboratory experiments conducted by some other investigators suggest that the unsteadiness of a tidal flow has a strong effect on the turbulent mechanism, but the logarithmic profile is still good in many cases (e.g., Wilkinson 1986; Anwar 1981,1983). By using field data measured in Start Bay off the South Devon coast, Wilkinson (1983) compared fitting results of a logarithmic profile with the log-linear profile suggested by Soulsby and Dyer (1981). He found that differences between quasisteady and unsteady theories were small, and that the roughness length was slightly higher than quasi-steady roughness length in an accelerating flow. He concluded that the accelerative effects were not important during the periods studied. However, his results showed that the bed roughness length z_0 increased systematically during the decelerating tidal phase from 0.5 to 1.3 cm. The fact that a lower value of z_0 was obtained in the accelerating flow and a higher value in the decelerating flow is consistent with the theory of Soulsby and Dyer for unsteady flow. It seems that acceleration effect still can not be neglected.

The laboratory experiments of an oscillation flow at the hydraulics Research Station conducted by Anwar (1981) showed that the logarithmic profile was still good to fit the velocity during accelerating and decelerating flow both in smooth bed and rough bed channels. According to the field measurements in the River Carron,

Scotland, Anwar (1983) found that the mean velocity profiles were log-linear in stratified flow, and logarithmic in well-mixed flow. He did find z_0 to increase with time in a decelerating flow in some measurements but to remain a constant value in some other measurements. He concluded that a large value of z_0 and its rapid rise were due to the bed form and to the sediment suspension.

From the above discussion, one can still argue about the use of a logarithmic velocity profile to estimate shear velocity and roughness length in an unsteady flow. No unified conclusion on the effects of flow acceleration and deceleration on turbulence parameters may be drawn. The reason could be differing conditions during measurements by different investigators, such as stratification, sediments resuspension or magnitude of flow acceleration, thus resulting in conflicting conclusions. It should be noted that the difference between estimated values in a logarithmic profile and direct measurements of Reynolds stress could be large (Gross and Nowell 1983) during an accelerating phase even when the logarithmic profile is a good to fit the velocity data in the least-square sense. As many investigators have suggested, it seems that further examination of the effects of acceleration on velocity profile both in field and laboratory is necessary.

With particular reference to tide-driven estuarine and coastal boundary layers, Soulsby (1983) and Dyer (1986) subdivide the bottom boundary layer into a bed layer, a constant stress layer, and an outer layer. The thickness of the constant stress layer is about 0.1-0.2δ, where δ is thickness of the bottom boundary layer. For an oscillatory flow, the thickness of the constant stress layer is much thinner than that in a steady flow. Thus applicability of equations (1.1.3) and (1.1.4) are restricted. In the outer layer, flow is highly affected by external conditions. The shear stress and turbulent energy diminishes towards the surface, and the velocity profile departs from the

logarithmic profile significantly. Gross and Nowell (1983) found that the velocity above the constant stress layer is larger than that estimated by the logarithmic profile. This feature was often found in depth-limited or pipe flow boundary layers (Hinze, 1975). Thus bottom shear stress will be overestimated when using equations (1.1.3) and (1.1.4) in the outer layer. In the prototype flow, slight curvature of the velocity profile (or departure from the logarithmic profile) is sometimes obvious but is more often hidden in the random error. Many measurements show that the velocity profile is often convex upwards (Dyer 1986). Since the lowest current observation is seldom closer than 15 cm to the bed, this curvature, if extrapolated towards the bed would calculate a larger shear stress and roughness height. Because it is difficult to determine the boundary between the outer layer and the constant stress layer, caution must be exercised when using equations (1.1.3) and (1.1.4) to estimate bottom stress.

Various velocity profiles measured experimentally over a smooth boundaries in the laboratory show that the velocity profile in the outer layer can be better represented by a power law distribution such as

$$\frac{u}{u_*} = 8.3(\frac{u_* z}{\nu})^{1/7}$$ (1.2.2)

where ν is kinematic viscosity. For a rough boundaries

$$\frac{u_1}{u_2} = \left(\frac{z_1}{z_2}\right)^{1/n}$$ (1.2.3)

where u_1 and u_2 are the velocities at elevation z_1 and z_2, n=5-10. In the situation where the boundary layer does not occupy the whole depth, velocity defect law is most applicable which gives

$$\frac{U_s - u}{u_*} = f\left(\frac{z}{\delta}\right)$$ (1.2.4)

where U_s is free stream velocity. However, these empirical equations do not directly relate to the universal logarithmic profile and give no information of bottom roughness so that their applicability is limited. These equations are occasionally used in the sea. The relationship between bottom stress and flow well above the bottom need to be resolved in the future.

1.3   Objectives of The Study

The purpose of the study is to investigate the effects of tidal flow acceleration and deceleration, and the effect of non-constant stress on the structure of bottom boundary layers, in particular, to investigate the near bottom velocity profile, the bottom stress, and their relationship to the flow above the bottom. A numerical model is used to simulate an estuarine bottom boundary layer and verify the analytical results. The specific objectives of the study are (1) to derive a theoretical formulation relating bottom shear stress to the flow acceleration as well as velocity in the bottom boundary layer, (2) to study the effects of acceleration on flow profile near the bottom and, in particular, to determine what deviations from the logarithmic profile are caused by acceleration and over what part of the tidal cycle, (3) to study the effect of non-constant stress on the near bottom velocity and the relationship between bottom stress and the flow above the bottom, and (4) to implement theoretical formulation in the numerical model to verify its applicability.

2. THEORETICAL ANALYSIS

2.1 Effect of Flow Acceleration

In lieu of equations (1.1.3) and (1.1.4), it is possible to derive a formulation to be used in a numerical model for specifying bottom stress in a homogeneous flow which includes the effect of flow acceleration. We consider a simple geometry channel with a very wide rectangular cross section. The channel is long enough that the local velocity profile becomes independent of the downstream distance x. As a result, the nonlinear inertial terms are also assumed negligible. This simplifies the theoretical analysis considerably and separates the bottom layer and outer layer problems from the problems associated with downstream development in other wall-bounded shear flows. Also, assuming bed is rough with hydraulic roughness height z_0 and no time-varying macroscale bed form, such as ripples, are formed on the bottom. We start with the unsteady boundary layer equation for homogeneous flow,

$$\frac{\partial u}{\partial t} = -\frac{1}{\rho}\frac{\partial p}{\partial x} + \frac{\partial \tau}{\partial z} \qquad (2.1.1)$$

where

  t is time,

  ρ is water density,

  p is pressure,

  x is distance along estuary axis, and

  τ is kinematic shear stress.

With the usual assumption that the horizontal pressure gradient is independent of z in

a thin boundary layer, equation (2.1.1) may be integrated with respect to z over the

bottom layer (figure 1) of a finite difference numerical model

$$\frac{\partial \bar{u}}{\partial t} = -\frac{1}{\rho}\frac{\partial p}{\partial x} + \frac{\tau_1 - \tau_b}{\Delta z} \qquad (2.1.2)$$

where $\bar{u}$ is the layer average velocity given by

$$\bar{u} = \frac{1}{\Delta z}\int_0^{\Delta z} u(z)dz$$

and τ_1 is the shear stress at height Δz. Subtracting equation (2.1.2) from equation

(2.1.1) gives

$$\frac{\partial u_d}{\partial t} = \frac{\partial}{\partial z}A_v\frac{\partial u_d}{\partial z} - \frac{\tau_1 - \tau_b}{\Delta z} \qquad (2.1.3)$$

where $u_d = u - \bar{u}$, is a function of z and Δz, and τ is related to eddy viscosity A_v by

$$\tau = A_v\frac{\partial u}{\partial z} = A_v\frac{\partial u_d}{\partial z}.$$

Assuming that A_v varies linearly with z, i.e., $A_v = A_0 z = \kappa u_* z$, where A_0 is only a

function of t, and defining $Z = z/\Delta z$, equation (2.1.3) becomes

$$\frac{\Delta z}{A_0}\frac{\partial u_d}{\partial t} = \frac{\partial}{\partial Z}(Z\frac{\partial u_d}{\partial Z}) - \frac{\tau_1 - \tau_b}{A_0}. \qquad (2.1.4)$$

Equation (2.1.4) in a full implicit three time level finite difference form, is

$$\frac{\Delta z}{2\Delta t A_0^{n+1}}(u_d^{n+1} - u_d^{n-1}) = \frac{\partial}{\partial Z}(Z\frac{\partial u_d^{n+1}}{\partial Z}) - \frac{1}{A_0^{n+1}}(\tau_1^{n+1} - \tau_b^{n+1}) \qquad (2.1.5)$$

where the superscript designates the time level.

Figure 1. Coordinate system and variables at the bottom layer of the computation grid in a numerical model.
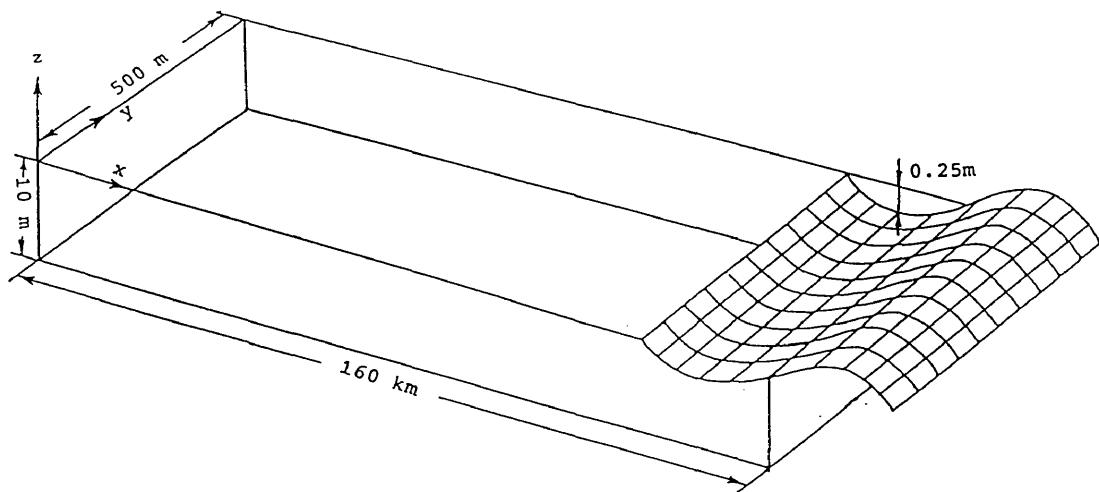
Figure 2. Sketch of a hypothetical estuary used in the model experiments.

With proper choices of Δz and Δt, we may define a small parameter $\xi = \Delta z/(2\, \Delta t\, A_0)$. Since ξ is a small parameter for tidal flow, the inertial term in equation (2.15) can be treated as a small perturbation. Using regular perturbation method, we express u_d^n and τ^n in terms of an infinite series in ξ,

$$u_d^n = \sum_{k=0}^{\infty} u_d^{k,n} \xi^k$$

$$\tau_l^n = \sum_{k=0}^{\infty} \tau_l^{k,n} \xi^k \qquad (2.1.6)$$

$$\tau_b^n = \sum_{k=0}^{\infty} \tau_b^{k,n} \xi^k$$

where superscripts 'k,n' for u_d, τ_l and τ_b designate the k-th order solution at time level n. Substituting into equation (2.1.5), the zero order equation becomes

$$\frac{\partial}{\partial Z}\left(Z\frac{\partial u_d^{0,n+1}}{\partial Z}\right) = \frac{1}{A_0^{n+1}}(\tau_l^{0,n+1} - \tau_b^{0,n+1}) \qquad (2.1.7)$$

with conditions:

$$A_0^{n+1} Z \frac{\partial u_d^{0,n+1}}{\partial Z}\Big|_{Z=1} = \tau_l^{0,n+1} \qquad (2.1.8)$$

$$u_d^{0,n+1}\Big|_{Z=z_o/\Delta z} = -\overline{u}^{0,n+1} \,. \qquad (2.1.9)$$

The no-slip condition is applied at the bottom and it is assumed that $z_0 \ll \Delta z$. Integrating equation (2.1.7) with boundary conditions and neglecting terms on the order of Z_0 gives

$$u_d^{0,n+1} = \frac{\tau_b^{0,n+1}}{A_0^{n+1}}\ln\left(\frac{Z}{Z_0}\right) - \overline{u}^{0,n+1} + \frac{\tau_l^{0,n+1} - \tau_b^{0,n+1}}{A_0^{n+1}}Z \,. \qquad (2.1.10)$$

Equation (2.1.10) results in a logarithmic velocity profile if a constant shear stress layer is assumed (i.e. $\tau_l^0 = \tau_b^0$), giving

$$u^{0,n+1} = \frac{\tau_b^{0,n+1}}{A_0^{n+1}} \ln(\frac{Z}{Z_0})$$

(2.1.10a)

or

$$u^{0,n+1} = \frac{u_*^{0,n+1}}{\kappa} \ln(\frac{z}{z_0}) \ .$$

(2.1.10b)

The first order terms in equation (2.1.5) give

$$\frac{\partial}{\partial Z}(Z\frac{\partial u_d^{1,n+1}}{\partial Z}) = \frac{\tau_1^{1,n+1} - \tau_b^{1,n+1}}{A_0^{n+1}} + u_d^{0,n+1} - u_d^{0,n-1}$$

(2.1.11)

with boundary conditions

$$A_0^{n+1} Z \frac{\partial u_d^{1,n+1}}{\partial Z} \Big|_{Z=1} = \tau_1^{1,n+1}$$

(2.1.12)

$$u_d^{1,n+1} \Big|_{Z=Z_0} = -\overline{u}^{1,n+1}$$

(2.1.13)

Here we also apply the no-slip condition at the bottom. Substituting equation (2.1.10) into (2.1.11) and integrating equation (2.1.11) vertically upwards from the bed gives

$$Z \frac{\partial u_d^{1,n+1}}{\partial Z} = \frac{\tau_1^{1,n+1} - \tau_b^{1,n+1}}{A_0^{n+1}} Z + (\frac{\tau_b^{0,n+1}}{A_0^{n+1}} - \frac{\tau_b^{0,n-1}}{A_0^{n-1}})(Z\ln(\frac{Z}{Z_0}) - Z) - (\overline{u}^{0,n+1} - \overline{u}^{0,n-1})Z +$$

$$(\frac{\tau_1^{0,n+1} - \tau_b^{0,n+1}}{A_0^{n+1}} - \frac{\tau_1^{0,n-1} - \tau_b^{0,n-1}}{A_0^{n-1}})\frac{Z^2}{2} + C_0 \ .$$

(2.1.14)

Using boundary condition (2.1.12) at Z=1 gives

$$C_0 = \frac{1}{A_0^{n+1}}\tau_b^{1,n+1} - (\frac{\tau_b^{0,n+1}}{A_0^{n+1}} - \frac{\tau_b^{0,n-1}}{A_0^{n-1}})(\ln(\frac{1}{Z_0})-1) + (\overline{u}^{n+1}-\overline{u}^{n-1})$$

$$-(\frac{\tau_1^{0,n+1}-\tau_b^{0,n+1}}{A_0^{n+1}} - \frac{\tau_1^{0,n-1}-\tau_b^{0,n-1}}{A_0^{n-1}})\frac{1}{2} \ . \tag{2.1.15}$$

Substituting C_0 into equation (2.1.14) gives

$$\frac{\partial u_d^{1,n+1}}{\partial Z} = \frac{\tau_1^{1,n+1}-\tau_b^{1,n+1}}{A_0^{n+1}} + [\ln(\frac{Z}{Z_0})-1-(\ln(\frac{1}{Z_0})-1)\frac{1}{Z}](\frac{\tau_b^{0,n+1}}{A_0^{n+1}} - \frac{\tau_b^{0,n-1}}{A_0^{n-1}})$$

$$-(1-\frac{1}{Z})(\overline{u}^{0,n+1}-\overline{u}^{0,n-1}) + \frac{\tau_b^{1,n+1}}{A_0^{n+1}Z} + (\frac{\tau_d^{0,n+1}}{A_0^{n+1}} - \frac{\tau_d^{0,n-1}}{A_0^{n-1}})(\frac{Z}{2}-\frac{1}{2Z}) \ , \tag{2.1.16}$$

where $\tau_d = \tau_1 - \tau_b$. Integrating equation (2.1.16) gives

$$u_d^{1,n+1} = \frac{\tau_1^{1,n+1}-\tau_b^{1,n+1}}{A_0^{n+1}}Z + (Z\ln(\frac{Z}{Z_0})-2Z-(\ln(\frac{1}{Z_0})-1)\ln Z)(\frac{\tau_b^{0,n+1}}{A_0^{n+1}} - \frac{\tau_b^{0,n-1}}{A_0^{n-1}})$$

$$-(Z-\ln Z)(\overline{u}^{0,n+1}-\overline{u}^{0,n-1}) + \frac{\tau_b^{1,n+1}}{A_0^{n+1}}\ln Z + (\frac{\tau_d^{0,n+1}}{A_0^{n+1}} - \frac{\tau_d^{0,n-1}}{A_0^{n-1}})(\frac{Z^2}{4}-\frac{1}{2}\ln(Z)) + C_1 \tag{2.1.17}$$

Using boundary condition (2.1.13) at $Z=Z_0$ results in

$$C_1 = -(\frac{\tau_1^{1,n+1}-\tau_b^{1,n+1}}{A_0^{n+1}})Z_0 + (2Z_0+(\ln(\frac{1}{Z_0})-1)\ln Z_0)(\frac{\tau_b^{0,n+1}}{A_0^{n+1}} - \frac{\tau_b^{0,n-1}}{A_0^{n-1}}) - \frac{\tau_b^{1,n+1}}{A_0^{n+1}}\ln(Z_0)$$

$$+(Z_0-\ln Z_0)(\overline{u}^{0,n+1}-\overline{u}^{0,n-1}) - (\frac{\tau_d^{0,n+1}}{A_0^{n+1}} - \frac{\tau_d^{0,n-1}}{A_0^{n-1}})[Z_0^2-\frac{1}{2}\ln(Z_0)] - \overline{u}^{1,n+1} \ , \tag{2.1.18}$$

Assuming $z_0 \ll \Delta z$ and substituting equation (2.1.18) into equation (2.1.17), the solution for $u_d^{1,n+1}$ may be obtained, which is combined with $\overline{u}^{1,n+1}$ to give

$$u^{1,n+1} = \frac{\tau_b^{1,n+1}}{A_0^{n+1}} \ln(\frac{Z}{Z_0}) + (\ln(\frac{Z}{Z_0}) - Z)(\overline{u}^{0,n+1} - \overline{u}^{0,n-1})$$

$$+ [\ln\frac{Z}{Z_0}(Z+1 -\ln\frac{1}{Z_0}) - 2Z](\frac{\tau_b^{0,n+1}}{A_0^{n+1}} - \frac{\tau_b^{0,n-1}}{A_0^{n-1}}) + \frac{1}{A_0^{n+1}}(\tau_1^{1,n+1} - \tau_b^{1,n+1})Z \qquad (2.1.19)$$

$$+ (\frac{Z^2}{4} - \frac{1}{2}\ln\frac{Z}{Z_0})(\frac{\tau_1^{0,n+1} - \tau_b^{0,n+1}}{A_0^{n+1}} - \frac{\tau_1^{0,n-1} - \tau_b^{0,n-1}}{A_0^{n-1}})$$

Assuming a constant stress layer and neglecting the second and higher order terms in ξ, the velocity profile may be written as

$$u^{n+1} = u^{0,n+1} + \xi u^{1,n+1}$$

or

$$u^{n+1} = u^{0,n+1} + \xi[\ln(\frac{Z}{Z_0})\frac{\tau_b^{1,n+1}}{A_0^{n+1}} + (\ln(\frac{Z}{Z_0}) - Z)(\overline{u}^{0,n+1} - \overline{u}^{0,n-1})$$

$$+ (\ln\frac{Z}{Z_0}(Z+1 -\ln\frac{1}{Z_0}) - 2Z)(\frac{\tau_b^{0,n+1}}{A_0^{n+1}} - \frac{\tau_b^{0,n-1}}{A_0^{n-1}})] \qquad (2.1.20)$$

Equation (2.1.19) may be used to calculate $\tau_b^{1,n+1}$ by setting Z at any value between Z_0 and 1 or integrating it from Z_0 to 1. Integrating equation(2.1.19) and neglecting terms on the order of Z_0, gives

$$\tau_b^{1,n+1} = A_0^{n+1}[\frac{1}{K_1}\overline{u}^{1,n+1} + K_2(\frac{\tau_b^{0,n+1}}{A_0^{n+1}} - \frac{\tau_b^{0,n-1}}{A_0^{n-1}}) + K_3(\overline{u}^{0,n+1} - \overline{u}^{0,n-1})] \qquad (2.1.21)$$

where

$$K_1 = \ln(\frac{1}{Z_0}) - 1$$

$$K_2 = \frac{3}{4K_1} + K_1 - \frac{1}{2}$$

$$K_3 = \frac{1}{2K_1} - 1 \quad .$$

Combining $\tau_b^{1,n+1}$ with $\tau_b^{0,n+1}$ gives

$$\tau_b^{n+1} = \tau_b^{0,n+1} + \xi \frac{A_0^{n+1}}{K_1} \bar{u}^{1,n+1} + \Delta z [K_2 \frac{(\tau_b^0/A_0)^{n+1} - (\tau_b^0/A_0)^{n-1}}{2\Delta t} + K_3 \frac{\bar{u}^{0,n+1} - \bar{u}^{0,n-1}}{2\Delta t}] \quad . \tag{2.1.22}$$

The zero order bottom stress, $\tau_b^{0,n+1}$, is related to the zero order velocity by integrating of equation (2.1.10a) from z_0 to Δz

$$\frac{\tau_b^{0,n+1}}{A_0^{n+1}} = \frac{\bar{u}^{0,n+1}}{\ln(\frac{1}{Z_0}) - 1} \quad . \tag{2.1.23}$$

Combining the first two terms on the right hand side of equation (2.1.22) by using equation (2.1.23) gives

$$\tau_b^{n+1} = \frac{A_0^{n+1} \bar{u}^{0,n+1}}{K_1} + \xi \frac{A_0^{n+1}}{K_1} \bar{u}^{1,n+1} + \Delta z [K_2 \frac{(\tau_b^0/A_0)^{n+1} - (\tau_b^0/A_0)^{n-1}}{2\Delta t} + K_3 \frac{\bar{u}^{0,n+1} - \bar{u}^{0,n-1}}{2\Delta t}]$$

$$= \frac{\kappa u_*^{n+1} \bar{u}^{n+1}}{K_1} + \Delta z [K_2 \frac{(\tau_b^0/A_0)^{n+1} - (\tau_b^0/A_0)^{n-1}}{2\Delta t} + K_3 \frac{\bar{u}^{0,n+1} - \bar{u}^{0,n-1}}{2\Delta t}]$$

or

$$\tau_b^{n+1} = \sqrt{C_D} |u_*^{n+1}| |\bar{u}^{n+1} + \Delta z [K_2 \frac{(\tau_b^0/A_0)^{n+1} - (\tau_b^0/A_0)^{n-1}}{2\Delta t} + K_3 \frac{\bar{u}^{0,n+1} - \bar{u}^{0,n-1}}{2\Delta t}] \quad , \tag{2.1.24}$$

or

$$u_*^{n+1} = \sqrt{C_D}\; \overline{u}^{n+1} + \frac{\Delta z}{u_*^{n+1}}[K_2 \frac{(\tau_b^0/A_0)^{n+1} - (\tau_b^0/A_0)^{n-1}}{2\Delta t} + K_3 \frac{\overline{u}^{0,n+1} - \overline{u}^{0,n-1}}{2\Delta t}]$$ (2.1.24a)

where

$$C_D = \frac{\kappa^2}{\left(\ln(\frac{1}{Z_0}) - 1\right)^2} \quad .$$

Equation (2.1.24a) shows that the bottom shear velocity consists of two parts. The first term on the right hand side of equation (2.1.24a) is the same formula as that commonly used to calculate shear velocity from a logarithmic velocity profile. The second term on the right hand side of the equation consists of the time derivatives of shear velocity and mean velocity over the first layer. It represents the effect of flow acceleration and is out of phase with the zero order bottom stress or velocity. Therefore, it is more important when the tidal flow changes direction and the bottom shear stress is small. When the flow acceleration is negligible, the second term will drop to zero so that equation (2.1.24) will reduce to the equation which is commonly used to calculate bottom shear stress from a logarithmic velocity profile.

The two parts in the last term of equation (2.1.24) may be combined into one by using equation (2.1.23). Substituting equations (2.1.23) into (2.1.24) gives

$$\tau_b^{n+1} = \sqrt{C_D}\; |u_*^{n+1}| |\overline{u}^{n+1} + \frac{3\Delta z}{4K_1^2} \frac{\overline{u}^{0,n+1} - \overline{u}^{0,n-1}}{2\Delta t} \quad .$$ (2.1.25)

We can simplify the velocity profile by substituting equations (2.1.10a) into equation (2.1.20) to give

$$u^{n+1} = \frac{\tau_b^{0,n+1}}{A_0^{n+1}}\ln(\frac{Z}{Z_0}) + \xi\frac{\tau_b^{1,n+1}}{A_0^{n+1}}\ln(\frac{Z}{Z_0}) +$$

$$\xi\left((\ln(\frac{Z}{Z_0})-Z)(\bar{u}^{0,n+1}-\bar{u}^{0,n-1}) + [\ln(\frac{Z}{Z_0})(Z+1-\ln\frac{1}{Z_0})-2Z](\frac{\tau_b^{0,n+1}}{A_0^{n+1}} - \frac{\tau_b^{0,n-1}}{A_0^{n-1}})\right) . \tag{1.2.26}$$

Combining the first two terms on the right hand side of the equation gives

$$u^{n+1} = \frac{u_*}{\kappa}\ln(\frac{Z}{Z_0}) +$$

$$\xi\left((\ln(\frac{Z}{Z_0})-Z)(\bar{u}^{0,n+1}-\bar{u}^{0,n-1}) + [\ln(\frac{Z}{Z_0})(Z+1-\ln\frac{1}{Z_0})-2Z](\frac{\tau_b^{0,n+1}}{A_0^{n+1}} - \frac{\tau_b^{0,n-1}}{A_0^{n-1}})\right) . \tag{2.1.26a}$$

Substituting equation (2.1.23) into equation (2.1.26a) and neglecting the second and higher order terms in ξ gives

$$u^{n+1} = \frac{u_*^{n+1}}{\kappa}\left(\ln(\frac{Z}{Z_0}) + \frac{\Delta z(\ln(Z)-1)}{\kappa}\frac{u_*^{n+1}-u_*^{n-1}}{2\Delta t(u_*|u_*|)^{n+1}}(Z-Z_0)\right) . \tag{2.1.27}$$

Equation (2.1.27) shows that velocity profile has two terms: the logarithmic profile and the first order correction term. The velocity deviates from the logarithmic velocity profile when flow acceleration is important. It is known from the derivation that the equation (2.1.27) is discontinuous at $u_*=0$. Thus, the equation is good only when u_* is not very close to zero. However, when u_* goes to zero, the velocity goes to zero too so that we may define that correction term equals zero if $|u_*|$ is less than a certain minimum value of the shear velocity. For comparison with previous results, it may be written in a time continuous form.

$$u = \frac{u_*}{\kappa}\left(\ln\frac{z}{z_0} - \frac{\Delta z(1-\ln(Z))}{\kappa}\frac{\partial_t u_*}{u_*|u_*|}(Z-Z_0)\right). \tag{2.1.28}$$

This formula is similar to the form proposed by Soulsby and Dyer (1981). But, besides the linear correction term, we have another correction term involving ZlnZ. To compare with their equation, lnZ is expanded about Z=1 in the range of Z<1 so that equation (2.1.28) can be written as

$$u = \frac{u_*}{\kappa}\left(\ln\frac{z}{z_0} - \frac{2}{\kappa}\frac{\partial_t u_*}{u_*|u_*|}(z-z_0) + \frac{\Delta z\partial_t u_*}{\kappa|u_*|u_*}Z^2\right). \tag{2.1.28a}$$

Comparing the coefficient of linear correction term with their equation, their empirical constant γ is equivalent to $\kappa/2$. Taking $\kappa=0.4$ gives $\gamma=0.2$. This value is close to the value of 0.3 estimated from the laboratory data of Jonsson and Carlsen (1976). However, the value of 0.2 is larger than that estimated from the field data, which varies from 0.02 to 0.236 and has an average value of 0.04 (Soulsby and Dyer 1981).

Equation (2.1.25) can be used to estimate the relative error of bottom shear velocity if acceleration effect is neglected. The relative error in the bottom shear velocity as a result of neglecting flow acceleration may be estimated as

$$\frac{u_*^{n+1}-\hat{u}_*^{0,n+1}}{u_*^{n+1}} = \frac{\Delta z}{\sqrt{C_d}\,|u_*^{n+1}|\,\overline{u}^{n+1}}\frac{3}{4K_L^2}\frac{\overline{u}^{0,n+1}-\overline{u}^{0,n-1}}{2\Delta t} \tag{2.1.29}$$

where

$$\hat{u}_*^{0,n+1} = \sqrt{C_D}\,\overline{u}^{n+1}.$$

Neglecting terms of second and higher order in ξ, $\bar{u}^0$ in equation (2.1.29) can be written in term of $\bar{u}$ giving

$$e = \frac{u_* - \hat{u}_*^0}{u_*} = \frac{3}{4}\eta \qquad (2.1.30)$$

where

$$\eta = \frac{\Delta z \partial_t \bar{u}}{\kappa^2 \bar{u}|\bar{u}|}$$

The relative error in the bottom shear stress as the result of neglecting acceleration may be estimated from the error of bottom shear velocity. From equation (2.1.30),

$$\hat{u}_*^0 = u_*(1 - \frac{3}{4}\eta) \qquad (2.1.31)$$

giving

$$(\hat{u}_*^0)^2 = u_*^2(1 - \frac{3}{2}\eta + \frac{9}{16}\eta^2) \ . \qquad (2.1.32)$$

letting

$$\hat{\tau}_b^0 = (\hat{u}_*^0)^2 = C_D|\bar{u}|\bar{u}$$

results an expression for the error.

$$e_b = \frac{\tau_b - \hat{\tau}_b^0}{\tau_b} = \frac{3}{2}\eta + \frac{9}{16}\eta^2 \qquad (2.1.33)$$

Equation (2.1.33) gives a simple formula to estimate the relative error due to missing acceleration effect. Taking a semidiurnal sinusoidal tide with peak average velocity at 1m above the bottom equals 0.15ms^{-1}, $\Delta z=1\text{m}$, and $\sigma=1.4\times10^{-4}\text{rad s}^{-1}$. Half hour after

slack water, the error is about 14%.

Equation(2.1.24a) gives the correction of acceleration effect for the shear velocity if roughness height is known. However, it is a common practice to calculate u_* and z_0 by best straight line fitting to the plot of $u(z)$ against $\ln z$. It is possible to find the relationship between the true u_*, z_0 and their estimated value from a best fit using equation (2.1.28a). Assuming z_1 and z_u are the lowest and uppermost measuring heights, respectively. The gradient of velocity profile corresponds roughly to the gradient of the profile at a height $z_m=(z_1 z_u)^{1/2}$. From equation (2.1.28a), the velocity gradient at $z=z_m$ is (neglecting the third term on the right hand side of the equation)

$$\frac{\partial u}{\partial z}=\frac{u_*}{\kappa z_m}\left(1-\frac{2}{\kappa}\frac{z_m\partial_t u_*}{u_*|u_*|}\right).$$

(2.1.34)

However, the velocity gradient at $z=z_m$ given by regression is

$$\frac{\partial u}{\partial z}=\frac{\bar{u}_*}{\kappa z_m}$$

(2.1.35)

where $\bar{u}_*$ is shear velocity estimated by best fitting. The estimated value $\bar{u}_*$ thus obtained in an accelerating flow is related to the true u_* by

$$\bar{u}_*=u_*(1-\frac{2\partial_t u_*}{\kappa|u_*|u_*}z_m)$$

(2.1.36)

or

$$\bar{\tau}=\tau(1-\frac{2\partial_t u_*}{\kappa|u_*|u_*}z_m)^2\approx\tau(1-\frac{4\partial_t u_*}{\kappa|u_*|u_*}z_m)$$

(2.1.36a)

where $\bar{\tau}$ is the shear stress estimated by regression.

We can also obtain the relation between true z_0 and its estimated value $\tilde{z}_0$. Again, neglecting the third term on the right hand side of the equation (2.1.28a) gives

$$\frac{u\kappa}{u_*} = \ln\frac{z_m}{z_0} - \frac{2}{\kappa}\frac{\partial_t u_*}{u_*|u_*|}z_m \ .$$

(1.2.37)

Equation (1.1.2) gives

$$\frac{u\kappa}{\tilde{u}_*} = \ln\left(\frac{z_m}{\tilde{z}_0}\right) \ .$$

(2.1.38)

Combing equations (2.1.37) and (2.1.38) gives

$$\frac{u\kappa}{u_*} - \frac{u\kappa}{\tilde{u}_*} + \frac{2z_m\partial u_*}{\kappa|u_*|u_*} = \ln\left(\frac{\tilde{z}_0}{z_0}\right) \ .$$

(2.1.39)

Using equation (2.1.34) and (2.1.36) gives

$$\tilde{z}_0 = z_0 \exp\left(\frac{\ln(z_m/z_0)-1}{1-\dfrac{\kappa|u_*|u_*}{2z_m\partial_t u_*}}\right) \ .$$

(2.1.40)

Taking a semidiurnal sinusoidal tide with peak shear velocity $u_* = 1.0$cm s^{-1}, $\sigma = 1.4 \times 10^{-4}$ rad s^{-1}, $z_0 = 0.1$cm and $z_m = 0.5$m, then 1 hour after slack water, the shear stress will be underestimated by 13% and the roughness height will be underestimated by 55%. If the same conditions are applied at 1 hour before slack water, the roughness height will be overestimated by 83%. Apparently, flow acceleration effect on estimated roughness heights is more significant than that on estimated shear stress in an unsteady flow. It

also indicates that changing roughness height during the tidal acceleration phase will be observed in the field if the regression method is applied to estimate it.

2.2 The Effect of Non-constant Stress

In the above discussion, a constant stress was assumed in the layer of thickness Δz. The assumption makes the mathematical derivation much simpler. However, the velocity will depart from the logarithmic profile in the outer layer even if flow acceleration is small. Therefore, some corrections for the effect of non-constant stress are necessary if the results derived under constant stress condition is applied to the elevation outside of the constant stress layer. One assumption which is made in the derivation of all the results in the previous section is a linear eddy viscosity distribution in the layer thickness Δz. It is questionable to apply this in the region of Δz when the thickness Δz is thicker than that of the constant stress layer. The linear assumption of eddy viscosity distribution overestimates the eddy viscosity in the outer layer so that the velocity gradient is underestimated. To improve accuracy of calculating bottom stress, a more complicated parameterization for eddy viscosity is necessary.

One formula for eddy viscosity used widely by many researchers (e.g. Arya 1973; Lundgren 1972; and Lavelle 1983) is

$$A_v = \kappa u_* z e^{-z/z_p}$$
(2.2.1)

In this form, the eddy viscosity increases linearly very near the bottom, reaches a maximum at z_p, and returns towards zero above far away from the bottom. It seems

more suitable than linear distribution. The height z_p is related to the constant stress layer height δ_c (e.g. Lavelle and Mofjeld 1983) by

$$z_p = e\delta_c \qquad (2.2.1a)$$

where $e=2.72$. Although equation (2.2.1) is more often used in deep flow where the surface is far removed from the turbulence generating region near the bottom, it is still a good approximation for near bottom eddy viscosity in an estuarine flow.

Assuming eddy viscosity has the form of equation (2.2.1) in the layer thickness of Δz near the bottom, the zero order problem of equation (2.1.7) becomes

$$\frac{\partial}{\partial z}\left(\kappa u_* z e^{-z/z_p}\frac{\partial u^0}{\partial z}\right) = \frac{\tau_1^0 - \tau_b^0}{\Delta z} \qquad (2.2.2)$$

The zero order problem is rewritten in dimensional form and the superscripts of time level, isomitted with variables understood to be at the present time level n+1. Integrating the rewritten equation (2.2.2) with respect to z from z_0 to Δz with the boundary condition

$$\left.\kappa u_* z e^{-z/z_p}\frac{\partial u^0}{\partial z}\right|_{z=\Delta z} = \tau_1^0$$

the velocity gradient is given by

$$\frac{\partial u^0}{\partial z} = \frac{1}{\kappa u_*}\left(\frac{\tau_1^0 - \tau_b^0}{\Delta z} + \frac{\tau_b^0}{z}\right)e^{z/z_p} \qquad (2.2.3)$$

In the region $z < z_p$, substituting

$$e^{-z/z_p} \approx 1 + \left(\frac{z}{z_p}\right) + \frac{1}{2}\left(\frac{z}{z_p}\right)^2 \tag{2.2.4}$$

into equation (2.2.3) and carrying out the integration gives

$$u^0 = \frac{u_*^0}{\kappa}\left(\ln\left(\frac{z}{z_0}\right) + L'\right) \tag{2.2.5}$$

where

$$L' = \frac{1}{z_p}(z - z_0) + \frac{1}{4z_p^2}(z^2 - z_0^2) + \frac{\tau_1^0 - \tau_b^0}{\tau_b^0}\left[\frac{z - z_0}{\Delta z} + \frac{z^2 - z_0^2}{2\Delta z z_p} + \frac{z^3 - z_0^3}{6\Delta z z_p^2}\right] \tag{2.2.6}$$

Equation (2.2.5) includes linear and the quadratic correction terms which increase as z increases. It will be shown later that the first order term is positive so that velocity is larger than that estimated by the logarithmic profile. The non-constant stress correction terms are in phase with the bottom velocity so that they are more important around the peak flow. Since linear assumption of eddy viscosity is good within the constant stress layer. Equation (2.2.5) should reduce to the logarithmic profile if $z \leq \delta_c$, i.e. requiring $\delta_c / z_p \ll 1$. Lavelle and Mofjeld (1983) matched the maximum of the profile (2.2.1) with the value of linear eddy viscosity $A_v = \kappa u_* z$ at the thickness δ_c, i.e. $z_p = e\delta_c$, so that above condition is satisfied. Equation (2.2.5) is more suitable than the logarithmic function to describe the velocity profile in the outer layer.

Comparing the magnitudes of two linear terms with other terms on the right side of equation (2.2.6), the linear terms are the dominant terms. To the first order approximation, we may neglect other terms for the practical application. Equation (2.2.6) may be further simplified by evaluating τ_1^0 at $z = \Delta z$ using equation (2.2.5). After neglecting higher order terms, equation (2.2.5) gives

$$\frac{\partial u^0}{\partial z}\bigg|_{z=\Delta z} = \frac{u_*^0}{\kappa}\left(\frac{1}{\Delta z}+\frac{1}{z_p}+\frac{\tau_1^0-\tau_b^0}{\tau_b^0\Delta z}\right)$$ (2.2.7)

or

$$\tau_1^0=\tau_b^0\Delta z e^{-\Delta z/z_p}\left(\frac{1}{\Delta z}+\frac{1}{z_p}+\frac{\tau_1^0-\tau_b^0}{\tau_b^0\Delta z}\right)$$ (2.2.8)

Substituting equation (2.2.4), with $z=\Delta z$, into equation (2.2.8) gives

$$\tau_1^0=\frac{1}{1+\dfrac{\Delta z}{2z_p}}\tau_b^0$$ (2.2.9)

Substituting (2.2.9) into (2.2.6), and retaining the linear term only, gives

$$L'=\frac{1}{2z_p}(z-z_0)$$ (2.2.10)

Therefore, from equation (2.2.5), the modified drag coefficient can then be written as

$$C'_D=\frac{\kappa^2}{\left(\ln(\dfrac{z}{z_0})+\dfrac{1}{2z_p}(z-z_0)\right)^2}$$ (2.2.11)

and

$$(u_*^0)^2=C'_D(u^0)^2$$

Equation (2.2.11) can be used to estimate the bottom stress from measured velocity data if the parameter z_p or the thickness of the constant stress layer δ_c can be estimated from the data. The thickness of the constant stress layer is very difficult to

measure. Under the assumption of linear eddy viscosity, steady flow is logarithmic to height δ_c when

$$\frac{\delta_c/H}{\ln(\delta_c/z_0)} < 1 \qquad (2.2.12)$$

(e.g., Lavell and Mofjeld, 1983), where H is total water depth. In a pure oscillatory flow the boundary layer thickness (Dyer 1986)

$$\delta = \frac{u_{*m}}{\sigma} \qquad (2.2.13)$$

where u_{*m} is the maximum shear velocity , and σ is the angular frequency of the oscillation. The constant stress layer has a thickness of $0.1-0.2\delta$. However, the boundary layer may not be fully developed in the depth limited environment and equation (2.2.13) may not give applicable estimation in shallow water. Based on the steady flow result and the boundary layer thickness of a pure oscillatory flow, the thickness of a constant stress layer dependents on the characteristic of bottom shear velocity, the characteristic frequency of motion σ. Lavelle and Mofjeld (1983) suggested that the thickness of a constant stress layer is given by

$$\delta_c = \frac{<|u_*|>^2}{\sigma u_s} \qquad (2.2.14)$$

where $<|u_*|>$ is tidal average of absolute shear velocity and u_s is the amplitude of the free-stream velocity, thus equation (2.2.14) gives the mean thickness of the constant stress layer. It shows that the thickness of the constant stress layer decreases with the frequency of motion and increases with roughness height. We can expect that the thickness of the constant stress layer in an unsteady flow is much thinner than that in a steady flow. Therefore, the correction for non-constant stress is necessary when

using large vertical grid spacing in a numerical model.

Comparing the magnitude of correction terms with the logarithmic term in equation (2.2.5), the magnitude of correction terms are smaller than that of the logarithmic term when $z<z_p$. If substituting equation (2.2.5) into the first order problem of equation (2.1.11), the non-constant stress correction terms will reduce to the second order terms, and is thus negligible. Therefore, it is necessary to include the non-constant stress correction in the zero order solution and combine it with equation (2.1.25) to arrive at

$$\tau_b^{n+1} = \sqrt{\tilde{C}_D} \, |u_*^{n+1}| \, |\overline{u}^{n+1} + \frac{3\Delta z}{4K_1^2} \frac{\overline{u}^{0,n+1} - \overline{u}^{0,n-1}}{2\Delta t}$$ (2.2.15)

where C_D is obtained by integrating equation (2.2.5) from z_0 to Δz, i.e.

$$\tilde{C}_D = \frac{\kappa^2}{\left(\ln(\frac{\Delta z}{z_0}) - 1 + \frac{\Delta z}{4z_p}\right)^2} \, .$$ (2.2.16)

Since the choice of the value for z_p and δ_c is quite empirical, it needs to be further verified in future studies. In a numerical model, however, z_p can be estimated from the values calculated in the model. Since maximum deviation from a logarithmic profile occurs around the peak flow, we may use values of u and u* at the peak of the previous tidal cycle to estimate z_p and use it for the present tidal cycle. If we only consider linear correction terms and neglect other terms as well as acceleration term (which is minimum at the peak flow), equation (2.2.5) can be written as

$$u_m^n = \frac{u_{*m}^n}{\kappa}\left(\ln\left(\frac{z}{z_0}\right) + \frac{1}{2z_p^n}(z-z_0)\right)$$ (2.2.17)

where u_m^n and u_{*m}^n are the maximum velocity and shear velocity, respectively, and superscript n designates the time level. Integrating equation (2.2.17) from z_0 to Δz gives

$$\frac{u_{1m}^n}{u_{*m}^n} - \frac{1}{\kappa}\left(\ln\left(\frac{\Delta z}{z_0}\right) - 1\right) = \frac{\Delta z}{4\kappa z_p^n} \qquad (2.2.18)$$

where u_{1m} is the maximum bottom average velocity at the first layer. Then z_p^{n+1} can be estimated by

$$z_p^{n+1} = \frac{\Delta z}{4\kappa}\left(\frac{u_{1m}^n}{u_{*m}^n} - \frac{1}{\kappa}\left(\ln\left(\frac{\Delta z}{z_0}\right) - 1\right)\right)^{-1} . \qquad (2.2.19)$$

When implementing equation (2.2.15) into a numerical model, the drag coefficient in equation (2.2.15) is substituted by equation (2.2.16) with z_p estimated from equation (2.2.19).

3.MATHEMATICAL MODEL

3.1   Model Formulation

The model experiments use a three dimensional hydrodynamic numerical model developed at VIMS by Hamrick (1992). The numerical model solves the vertically hydrostatic, free surface, variable density, turbulent averaged equations of motion and transport equations for turbulent kinetic energy and macroscale, salinity and temperature in a stretched, (sigma), vertical coordinate system, and horizontal coordinate systems which may be Cartesian or curvilinear-orthogonal. The details of the model are given in Hamrick (1992) and will not be reiterated here, with the exception of an outline of the governing equation.

The model formulates the equations by introducing both horizontal curvilinear and vertical stretching coordinates. The stretching is given by

$$z = (z^* + h)/(\zeta + h)$$

where z* denotes the original physical vertical coordinates and -h and ζ are the physical vertical coordinates of bottom topography and free surface respectively.

Transforming the vertically hydrostatic form of the equations of motion, and utilizing the Boussinesq approximation for variable density, results in the momentum and continuity equations and transport equations for salinity and temperature in the

following form (Hamrick, 1992):

$$\partial_t(mHu) + \partial_x(m_y Huu) + \partial_y(m_x Huv) + \partial_z(mwu) - (mf + v\partial_x m_y - u\partial_y m_x)Hv$$

$$= -m_y H\partial_x(g\zeta + p) - m_y(\partial_x h - z\partial_x H)\partial_z p + \partial_z(mH^{-1}A_v\partial_z u) + Q_u \tag{3.1.1}$$

$$\partial_t(mHv) + \partial_x(m_y Huv) + \partial_y(m_x Hvv) + \partial_z(mwv) + (mf + v\partial_x m_y - u\partial_y m_x)Hu$$

$$= -m_x H\partial_y(g\zeta + p) - m_x(\partial_y h - z\partial_y H)\partial_z P + \partial_z(mH^{-1}A_v\partial_z v) + Q_v \tag{3.1.2}$$

$$\partial_z p = -gH(\rho - \rho_0)\rho_0^{-1} = -gHb \tag{3.1.3}$$

$$\partial_t(m\zeta) + \partial_x(m_y Hu) + \partial_y(m_x Hv) + \partial_z(mw) = 0 \tag{3.1.4}$$

$$\partial_t(m\zeta) + \partial_x(m_y H\int_0^1 u\,dz) + \partial_y(m_x H\int_0^1 v\,dz) = 0 \tag{3.1.5}$$

$$\rho = \rho(p,s,T) \tag{3.1.6}$$

$$\partial_t(mHS) + \partial_x(m_y HuS) + \partial_y(m_x HvS) + \partial_z(mwS) = \partial_z(mH^{-1}A_b\partial_z S) + Q_s \tag{3.1.7}$$

$$\partial_t(mHT) + \partial_x(m_y HuT) + \partial_y(m_x HvT) + \partial_z(mwT) = \partial_z(mH^{-1}A_b\partial_z T) + Q_T \tag{3.1.8}$$

In these equations, u and v are the horizontal velocity components in the curvilinear, orthogonal coordinates x and y, m_x and m_y are the square roots of the diagonal components of the metric tensor and $m = m_x m_y$ is the Jacobian or square root of the metric tensor determinant. The total depth, $H = h + \zeta$, is the sum of the depth below and the free surface displacement relative to the undisturbed physical vertical coordinate origin, $z^* = 0$. The pressure p is the physical pressure in excess of the reference density

hydrostatic pressure $\rho_0 gH(1-z)$, divided by the reference density, ρ_0. f is the Coriolis parameter, A_v is the vertical turbulent or eddy viscosity, and Q_u and Q_v are momentum source-sink terms. The density, ρ, is in general a function of salinity, S, and temperature, T, and can be weak function of pressure, consistent with the incompressible continuity equation under the anelastic approximation. The buoyancy, b, is defined in equation (3.1.3) as the normalized deviation of density from the reference value. The continuity equation (3.1.4) has been integrated with respect to z over the interval (0,1) to produce the depth integrated continuity equation (3.1.5) using the vertical boundary condition, w=0, at z=(0,1). In the transport equations for salinity and temperature (3.1.7) and (3.1.8) the source and sink terms, Q_s and Q_T, include subgrid scale horizontal diffusion and thermal sources and sink, while A_b is the vertical turbulence diffusivity. The vertical velocity, with physical units, in the stretched, dimensionless vertical coordinate z is w, is related to the physical vertical velocity w^* by

$$w = w^* - z(\partial_t \zeta + u m_x^{-1} \partial_x \zeta + v m_y^{-1} \partial_y \zeta) + (1-z)(u m_x^{-1} \partial_x h + v m_y^{-1} \partial_y h) \qquad (3.1.9)$$

To provide the vertical turbulent viscosity and diffusivity, the second moment turbulence closure model developed by Mellor and Yamada(1982) and modified by Galperin et. al. (1988) is introduced. The model relates the vertical turbulent viscosity A_v and diffusivity A_b to the turbulent intensity, q , a turbulent length scale, l, and a Richardson number R_q, by

$$A_v = \phi_v q l = 0.4(1+36R_q)^{-1}(1+6R_q)^{-1}(1+8R_q)q l \qquad (3.1.10)$$

$$A_b = \phi_b q l = 0.5(1 + 36 R_q)^{-1} q l \tag{3.1.11}$$

$$R_q = \frac{g H \partial_z b l^2}{q^2 H^2} \tag{3.1.12}$$

The turbulence intensity and the turbulence length scale are determined by a pair of transport equations:

$$\partial_t(mHq^2) + \partial_x(m_y Huq^2) + \partial_y(m_x Hvq^2) + \partial_z(mwq^2) = \partial_z(mH^{-1}A_q \partial_z q^2) + Q_q$$

$$+ 2mH^{-1}A_v((\partial_z u)^2 + (\partial_z v)^2) + 2mg A_b \partial_z b - 2mH(B_1 l)^{-1} q^3 \tag{3.1.13}$$

$$\partial_t(mHq^2 l) + \partial_x(m_y Huq^2 l) + \partial_y(m_x Hvq^2 l) + \partial_z(mwq^2 l) = \partial_z(mH^{-1}A_q \partial_z q^2 l) + Q_l$$

$$+ mH^{-1}E_1 l A_v((\partial_x u)^2 + (\partial_z v)^2) + mg E_1 E_3 l A_b \partial_z b - mHB_1^{-1}q^3(1 + E_2(kL)^{-2}l^2) \tag{3.1.14}$$

$$L^{-1} = H^{-1}(z^{-1} + (l-z)^{-1}) \tag{3.1.15}$$

where B1, E1, E2, and E3 are empirical constants and Q_q and Q_l are additional source-sink terms such as subgrid scale horizontal diffusion. The vertical diffusivity, A_q, is taken equal to the vertical turbulent viscosity A_v.

3.2 Description of The Numerical Solution Technic

The numerical model uses a three time level, finite difference scheme with an internal-external mode splitting procedure to separate the internal shear or baroclinic mode from the external free surface gravity wave or barotropic mode. The external mode solution is fully implicit, and simultaneously computes the two-dimensional surface elevation field by a multicolor conjugate gradient solution procedure. The external solution is completed by the calculation of the depth averaged barotropic velocities using the new surface elevation field. The implicit external solution allows large time steps which are constrained only by the stability criteria of the explicit advection scheme used for the nonlinear accelerations.

The internal solution, at the same time step as the external, is implicit with respect to vertical diffusion. The internal solution of the momentum equations is in terms of the velocity shear, which results in the simplest and most accurate form of the baroclinic pressure gradients and eliminates the over determined character of alternate internal mode formulations. The vertical diffusion coefficients for momentum, mass and temperature are determined by the second moment closure scheme of Mellor and Yamada (Mellor and Yamada, 1982, and Galperin, et. al, 1988) which involves the use of analytically determined stability functions and the solution of transport equations for the turbulent kinetic energy and the turbulent macroscale. Numerical instability inherent to the three time level scheme is controlled by periodic insertion of a two time level step. The two time level step may also be used for startup and restart, eliminating the need for initial conditions at two time levels. A complete description of the theoretical and computational aspects of numerical scheme are presented in Hamrick (1992).

3.3 Treatment of Bottom Boundary conditions

The bottom boundary conditions for turbulence intensity and length scale are

$$q_b^2 = B_1^{2/3} |\tau_b|$$ (3.3.1)

$$l_b = 0$$ (3.3.2)

The bottom boundary condition for bottom stress with corrections for the effects of acceleration and non-constant stress is given by equations (2.2.15) and (2.2.16)

$$\tau_b^{n+1} = \sqrt{\tilde{C}_D} \, |u_*^{n+1}| \, |u_1^{n+1}| + \frac{3\Delta z}{4K_1} \frac{u_1^{0,n+1} - u_1^{0,n-1}}{2\Delta t}$$ (3.3.3)

where

$$\tilde{C}_D = \frac{\kappa^2}{\left(\ln(\frac{\Delta z}{z_0}) - 1 + \frac{\Delta z}{2z_p^{n+1}} \right)^2}$$ (3.3.3a)

$$K_1 = \ln\left(\frac{\Delta z}{z_0}\right) - 1$$ (3.3.4)

where u_1^0 is the zero order average velocity over the first layer. To implement equation (3.3.3) in a numerical model, the value of each term in the right hand side of the equation needs to be evaluated in terms of quantities available in the model. Thus u_*^{n+1} on the right hand side of the equation (3.3.3) may be substituted with u_*^n, i.e, a semi-explicit approach. Since the last term is the first order term of ζ, Δu_1^0 may be substituted by Δu_1. The difference $\Delta u_1 - \Delta u_1^0 = \zeta \Delta u_1^1$ is a second order term, thus negligible. The computation formula can, then, be written as

$$\tau_b^{n+1} = \sqrt{\tilde{C}_D} \, |u_*^n| |u_1^{n+1}| + \frac{3\Delta z}{4K_1^2} \frac{u_1^{n+1} - u_1^{n-1}}{2\Delta t} \tag{3.3.5}$$

where

$$\tilde{C}_D = \frac{\kappa^2}{\left(\ln(\frac{\Delta z}{z_0}) - 1 + \frac{\Delta z}{4z_P^{n+1}} \right)^2} \tag{3.3.5a}$$

$$z_P^{n+1} = \frac{\Delta z}{4\kappa} \left(\frac{u_{1m}^n}{u_{*m}^n} - \frac{1}{\kappa} \left(\ln\left(\frac{\Delta z}{z_0}\right) - 1 \right) \right)^{-1} \tag{3.3.5b}$$

where u_{1m}^n and u_{*m}^n are maximum bottom velocity and shear velocity in the previous tidal cycle.

Equation (3.3.5) can be directly implemented in the model to solve the internal model implicitly. This allows large time steps so that the restriction for ξ will be easily satisfied. The computation equation for the internal mode is written in terms of τ_{xz} (Hamrick, 1992)

$$-\Delta_k^{-1} \Delta_{k+1,k}^{-1} (\tau_{xz})_{k-1}^{n+1} + \left(\Delta_k^{-1} \Delta_{k+1,k}^{-1} + \frac{(H^u)^{n+1}}{2\Delta t} \left(\frac{H^u}{A_v^u} \right)^u + \Delta_{k+1}^{-1} \Delta_{k+1,k}^{-1} \right) (\tau_{xz})_k^{n+1} - \Delta_{k+1}^{-1} \Delta_{k+1,k}^{-1} (\tau_{xz})_{k+1}^{n+1}$$

$$= (2\Delta t \Delta_{k+1,k} m_y^u)^{-1} (u_{k+1} - u_k)^{**} \tag{3.3.6}$$

where H is water depth; Δ_k is the thickness of the k-th layer; $\Delta_{k+1,k} = 0.5(\Delta_{k+1} + \Delta_k)$; superscript '**' denotes the middle time level; u_k is the velocity at the level k. τ_{xz} is the shear stress. The bottom stress can be written as

$$(\tau_{xz})_0^{n+1} = \tau_b^{n+1} = \left(\sqrt{\bar{C}_D} \, |u_*^n| + \frac{3\Delta z}{2\Delta t} \frac{1}{4K_1^2} \right) u_1^{n+1} - \frac{3\Delta z}{2\Delta t} \frac{1}{4K_1^2} u_1^{n-1} \tag{3.3.7}$$

where u_1^{n+1} can be expressed in terms of the depth integrated transports and the internal shear stress by

$$u_1^{n+1} = \left(\frac{U}{m_y^u H^u} \right)^{n+1} - \sum_{k=1}^{K-1} \left(1 - \sum_{j=1}^{K} \Delta_j \right) \frac{\Delta_{k+1,k}(\tau_{xz})_k^{n+1}}{\left(\dfrac{A_v^u}{H^u} \right)_k^u} \tag{3.3.8}$$

Substitute equations (3.3.7) and (3.3.8) into equation (3.3.6), equation (3.3.6) can be used to solve τ_{xz} implicitly.

4. MODEL EXPERIMENTS WITH A HOMOGENEOUS FLOW

4.1 Model Conditions

A hypothetical estuary is used for numerical experiments. The physical problem for the model experiments is the reflection of a tidal wave propagation into a closed-end channel of uniform rectangular cross-section (figure 2). The parameters used in the model experiments with an M_2 and an M_8 tides are

M_2 tide:

  length of the channel = 160 km;

  depth of the channel = 10 m;

  width = 500 m;

  Δx = 5000 m;

  fresh water input = 0;

  period of tidal wave = 12.42 hour; and

  time step Δt = 310.5 seconds.

M_8 Tide:

  length of the channel = 40 km;

  depth of the channel = 10 m;

  width = 500 m;

$\Delta x = 1250$ m;

fresh water input = 0;

period of tidal wave = 3.105 hour; and

time step $\Delta t = 155.2$ seconds.

The model was applied in a two-dimensional fashion with a computational grid in longitudinal and vertical directions. Constant grid spacings were used, in vertical and longitudinal directions respectively, to avoid error introduced by uneven grid spacing. The oceanic salinity was set to zero in all depths so that salinity effects were not included in the tidal dynamics.

4.2 Test Runs

To assure our physical problem had been simulated correctly, several computational tests with the M_2 tide were conducted to exam the one dimensional and vertical two dimensional features of estuarine flow .

One dimensional features of the estuarine flow were tested by specifying the amplitude of incoming tidal wave 0.4m at the mouth. The model was run with 100 layer resolution. All computations were started with initial conditions of zero velocity and zero tidal height throughout the channel. The computation proceeded with simple harmonic forcing at the mouth, while the velocity at the closed end of the channel was kept at constant zero. The log-linear velocity profile with corrections for acceleration and non-constant stress effects was used to calculate bed shear stress as the bottom boundary condition (equation 3.3.5). Three roughness heights introduced in the test

runs were z_0=0.1, 0.5, 1.0cm, respectively. The model was run for 20 tidal cycles and the tidal amplitude and amplitude of surface velocity of the last tidal cycle were compared with theoretical curves based on the linear frictionless model. The model results of tidal amplitude and current amplitude are shown in figures 3 and 4, respectively. The results show that the feature of wave propagation and reflection is well simulated. As bottom roughness increases, tidal current amplitude decreases. The nodal point is located at 110 km from the head. The tidal amplitude decreases as bottom roughness increases at the upriver side of the nodal point, while tidal amplitude increases as bottom roughness increases at the downriver side of the nodal point.

To test two dimensional features of vertical structure in estuarine flows, the model was run with 100 layer vertical resolution i.e., average Δz=10cm. The boundary condition of bottom shear stress was calculated with and without corrections for acceleration and non-constant stress. The 'without correction' case assumes a logarithmic velocity profile and uses equation (1.1.5) to calculate bottom shear stress from the velocity at the 1st layer from the bottom, i.e. 5cm above the bottom. The 'with correction' case uses equation (3.3.5) to calculate bottom stress. Both cases were run by specifying tidal amplitude of 0.25m at the mouth and a constant roughness of 0.2cm throughout the channel. After 20 tidal cycles, the model reached equilibrium state. The results of the last tidal cycle were used to do the comparison. The results of the two cases are essentially the same since Δz is so small that the correction terms are negligible. Because the solutions of the 100 layer models with and without corrections are essentially the same, they can be considered as true representation of prototype flow structure. Figure 5 shows the velocity profile at different phases of the tide from maximum flood to maximum ebb (phases are referred to the velocity near the bottom). It shows the common feature of phase lead near the bottom boundary.

Figure 6 shows the vertical distribution of eddy viscosity at different phases of tide from maximum flood to maximum ebb velocity. The eddy viscosities reach maximum at certain level and diminish toward the surface and the bottom. This feature shows the common characteristic of eddy viscosity in an oscillatory boundary layer.
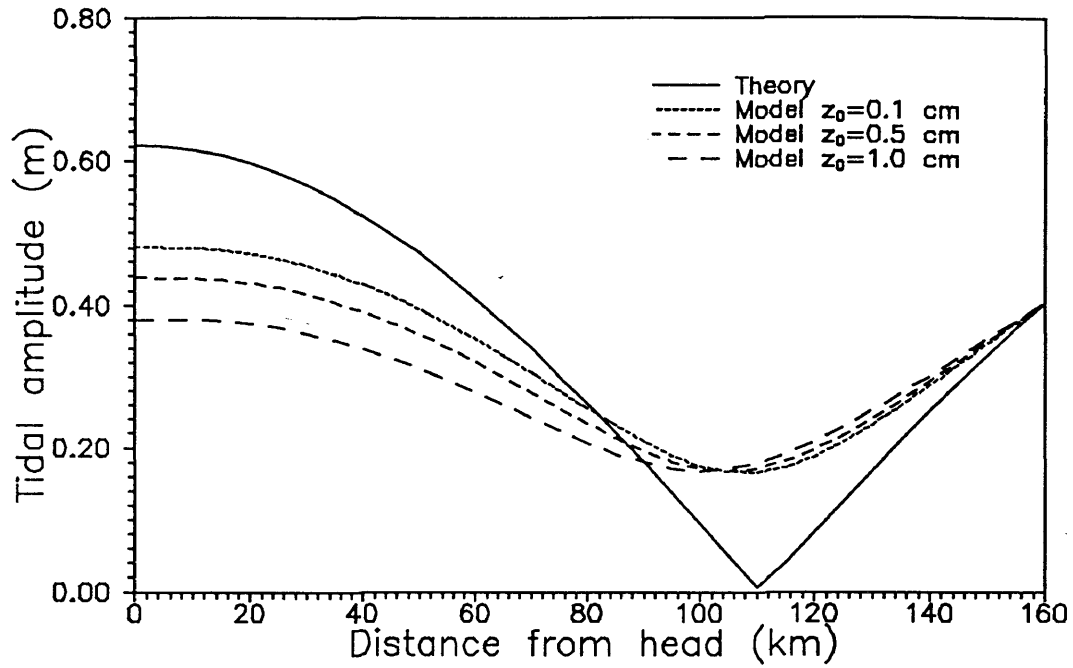
Figure 3. Distribution of tidal amplitude of an M_2 tide along the channel.
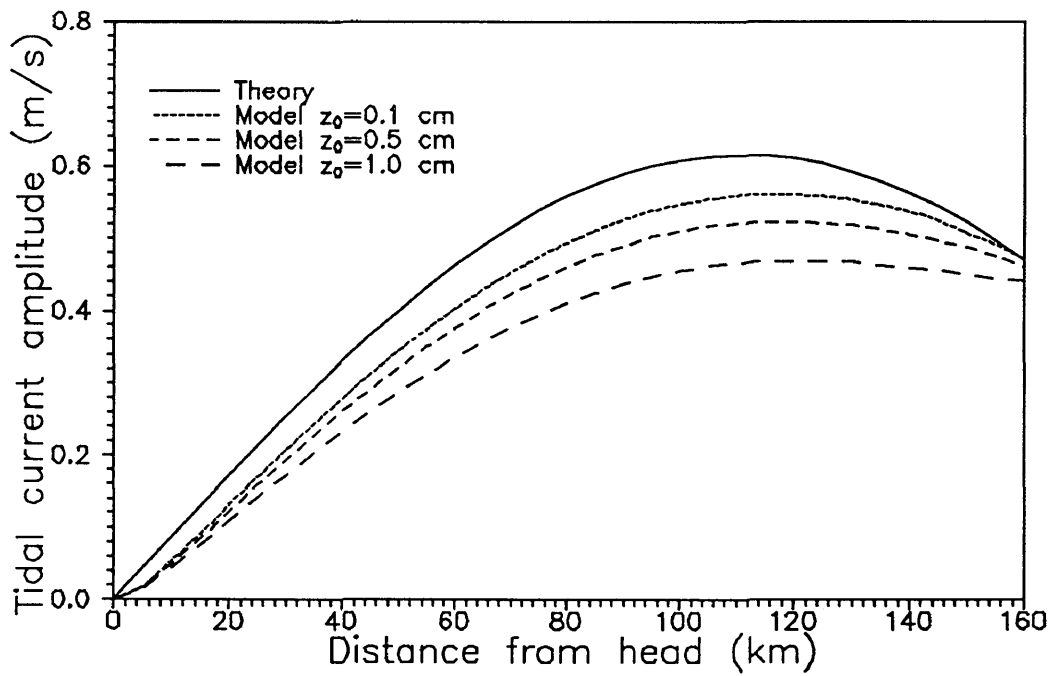
Figure 4. Distribution of current amplitude of an M_2 tide along the channel.
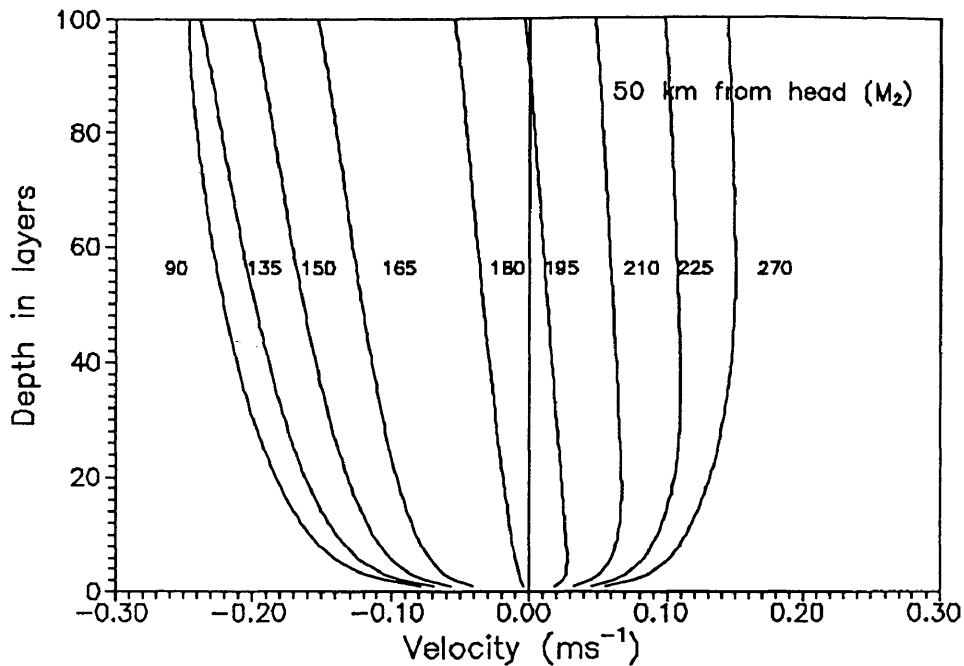
Figure 5.   Vertical velocity profiles calculated with 100
            layer model (The number for each curve represents
            tidal phase in degree, 90 degree is maximum flood).
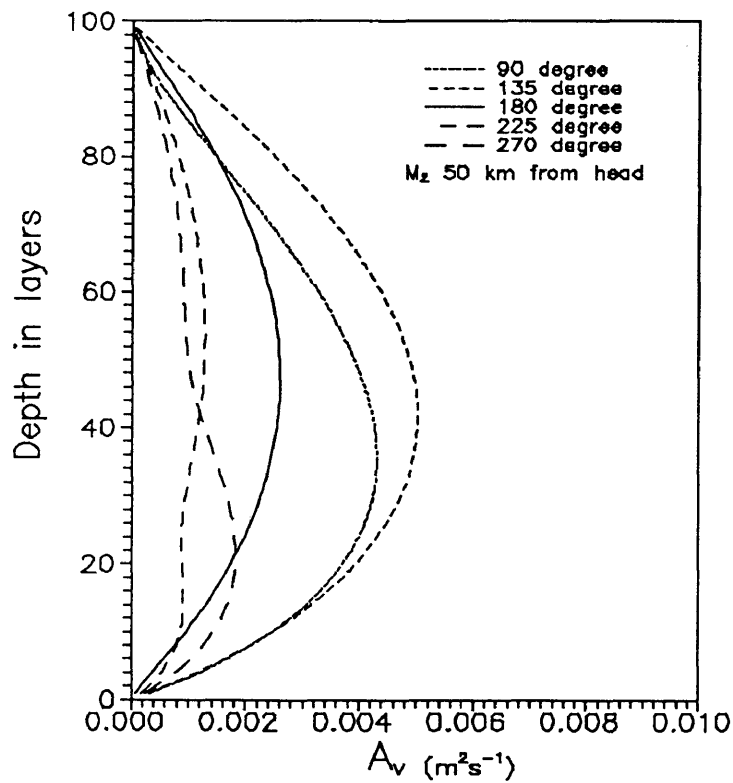
Figure 6.   Vertical distribution of eddy viscosity calculated
            from 100 layer model at 50 km from mouth (M_2
            tide, 90 degree is maximum flood).

4.3   Experiments with an M_2 Tide

The numerical model experiments with an M_2 tide were conducted by specifying an incoming tide of 0.25m amplitude at the mouth and a constant bottom roughness of 0.2cm throughout the channel. The model was run with 100 layer resolution and used equation (3.3.5) to specify the bottom stress since the use of equations (1.1.3) and (1.1.4) to specify bottom stress gives essentially the same results. Figure 7 presents the vertical non-dimensional velocity profiles at different phases of the tide. Comparing these with the logarithmic profile, the velocity profiles at different phases all show the logarithmic dependence near the bottom, except the profile at the very early stage of flow acceleration (195 degrees in figure 7). Velocity profiles deviate significantly from the logarithmic profile at the elevation 1m above the bottom. As the elevation increases, the deviation becomes more and more pronounced. The velocities are lower than those estimated by the logarithmic profile when flow is accelerating (195, 210 and 225 degrees) at the elevation far away from the bottom, i.e. the velocity profiles shift toward left from the logarithmic profile. Velocities are higher than those estimated by the logarithmic profile when flow is decelerating (150 and 165 degrees), i.e. the velocity profiles shift toward right from the logarithmic profile. This characteristic agrees with that described by equation (2.1.28). The characteristic of the flow during acceleration indicates that, away from the bed, the importance of inertia relative to frictional effects is greater than that near the bed, so that the flow well away from the boundary will retain a 'memory' longer than that near the bed. It can be expected that using logarithmic velocity profile to calculate bottom stress will underestimate the true bottom stress when flow is accelerating (e.g. 195 degrees) and overestimate the bottom stress when flow is decelerating (e.g. 165 degrees). The

maximum acceleration effect occurs around the slack tide. However, the duration of acceleration is relatively short, about 1 to 2 hours, comparing with tidal period. The acceleration effects gradually diminish as velocity increases towards maximum flood or ebb. Around the peak current, however, the velocity profiles all shift toward the right from the logarithmic profile as elevation increases (90 and 270 degrees in figure 7), i.e., the velocities are larger than those estimated by the logarithmic profile. As the elevation increases, the departure become more and more significant. This feature agrees with the velocity structure described by equation (2.2.5) which shows the non-constant stress effect on the velocity profile. This phenomenon was often observed in the depth-limited flow (e.g. Gross and Nowell, 1983). The thickness of the logarithmic layer is much thinner in an oscillatory flow than that in a steady flow because of inertia and non-constant stress effects.

With the solution from the numerical computation, we can investigate the bottom shear stress calculated from near bottom velocities assuming a logarithmic velocity profile. Figure 8 shows the bottom shear stresses calculated from the velocities at various heights above the bottom with equations (1.1.3) and (1.1.4). In these calculations, the roughness height of 0.2cm used in the model was assumed known and used in equation (1.1.4). The bottom stress calculated from the 100 layer model is considered as the true value. It is seen that deviations from the true value increase when the velocities farther away from the bottom are used to calculate the bottom stress. The deviation during the period around slack tide is mainly the result of the inertia effect. The values calculated by the logarithmic velocity profiles are too small during flow acceleration and too large during flow deceleration. The deviation around peak current is mainly the effect of non-constant stress which always over estimates the bottom shear stress when the velocities in the outer layer are used to calculate the bottom stress.

In the prototype, it is a common practice to measure the velocity profile near the bottom and estimate the roughness height and bottom shear stress by fitting the measured values with a logarithmic profile. We also applied this procedure with the velocity data computed by the model. Figure 9 shows the bottom shear stress and roughness height computed in this fashion. The velocity data between z=15cm and 105cm were used in regression. Values are estimated by regression of all velocity values (total of 9) between the two heights or by fitting the two extreme values with a logarithmic profiles. Both fits produce essentially the same results and they differ substantially from the value computed by the model. The calculated value of z_0 is roughly constant, however it is much higher than 0.2cm, the value used by the model, for most of the tidal cycle. The value of z_0 increases as flow decelerates and decreases as flow accelerates. The value varies significantly around slack tide when the acceleration effect is important.

The accuracy of using logarithmic profile to calculate the drag coefficient and bottom shear stress depends on the phase of the tide and the elevation at which velocity is used to calculate the bottom stress. As long as a velocity close to the bottom is used, both inertia and non-constant stress effect are small and the logarithmic profile is a satisfactory approximation for bottom stress calculation. If velocity far away from the bottom is used, overestimated bottom stress and underestimated bottom stress will occur when flow is decelerating and accelerating, respectively. The magnitude of error increases with the elevation at which velocity is used to calculate bottom stress. If the elevation is far away from the bottom, the bottom stress calculated by the logarithmic profile will always overestimate the bottom stress when current speed is high. Therefore, caution must be exercised when using regression to estimate shear stress and bottom roughness. Significant error may exist even though the logarithmic profile is a good fit to the data in the least-square sense.

The regression results calculated above all have good fits in the sense of statistics, but significant error occurs. This feature was often found when using field measurements to calculate bottom stress (e.g. Gross and Nowell, 1983) since the lowest current data is seldom closer than 15cm to the bed. The overestimation of bottom stress around the peak current, which seems very pronounced in our results, is mainly affected by flow outside of the constant stress layer. Therefore, it is necessary to incoroporate correction terms to correct for non-constant stress as well as inertia effects when velocity far away from the bottom is used to calculate the bottom stress.

According to the model results, the amplitude of bottom shear velocity and surface velocity are 0.8cm s^{-1} and 25cm s^{-1}, respectively. For a semidiurnal sinusoidal tide, the thickness of the constant stress layer is about 0.74m (equation 2.2.14) and $z_p=e\delta_c=2\text{m}$. Figure 10 shows the results of bottom stresses calculated from the velocities at different heights by using the drag law together with modified drag coefficient C_D (equation 2.2.11). The results are quite satisfactory except during period around slack tide. Figure 11 compares the regression results, calculated from the logarithmic velocity profile and the log-linear velocity profile (equations 2.2.5 and 2.2.10), with model results. Both bottom stress and the roughness height calculated from the regression of data between 15cm and 105cm by using log-linear profile agree with the model results, except during the period around slack tide. Because the logarithmic term and linear term are highly correlated in the equation (2.2.5), the coefficients of the linear term is not statistically significant so that more error may be introduced for u_* when doing regression without specifying z_p. To obtain a good estimates of u_* and z_0, specifying z_p before regression is necessary. Since the log-linear profile only corrects the zero order solution, this provides good prediction only when flow acceleration is small. The deviation between bottom stress calculated from regression and the numerical model remain unchanged when flow is accelerating. Since the

choice of z_p is quite empirical, it needs to be further verified in future studies.

The magnitude of inertia effect depends on the acceleration parameter $\partial_t \bar{u}/\bar{u}^2$. The relative error of neglecting the inertia effect is a function of tidal frequency and tidal current amplitude. For a given frequency, lower tidal amplitude will result in a larger deviation (equation 2.1.30). Consequently, changing tidal amplitude will affect the vertical velocity profile and the thickness of the logarithmic layer. Two model experiments with tidal forcings amplitudes of 0.5m and 1.0m were conducted to examine the change vertical velocity profiles as tidal amplitudes change. Figures 12 (a) and (b) show the model results for vertical non-dimensional velocity profiles with tides of 0.5m and 1.0m amplitudes, respectively. Comparing these with figure 7, at a given elevation, the velocity deviates more from the logarithmic profile as tidal amplitude decrease. For instance, no significant deviation of velocity profiles occur at 1m from the bottom half hour after slack tide (195 degrees) when tidal amplitude equals 1m, while there is substantial deviation from the logarithmic profile at the same elevation and tidal phase when tidal amplitude is 0.25m. In other words, the relative error due to the inertia effect is depressed substantially as tidal amplitude increase.

For practical application to prototype estuaries, a numerical model with 100 layers is not feasible. If we apply the model with 10 layer vertical resolution (Δz=1m) to the hypothetical estuary, we can expect that the effect of correction terms for bottom shear stress will increase because of the larger Δz. Figure 13 compares the bottom shear stress calculated with 100 layer mode, and the 10 layer model with and without correction terms. The 'with correction' case uses equation (3.3.5). Though the computed bottom stress of the 10 layer model without correction terms differs only slightly from that of the 100 layer model, the deviation qualitatively agrees with the theoretical results of the previous sections. When the acceleration effect dominates, the

model with a large Δz underestimates the bottom stress during acceleration. The numerical model tends to reduce the effect of the correction terms because of negative feed back in the numerical computations. When the assumed logarithmic profile underestimates the bottom stress, the model will overestimate the near bottom velocity. It in turn will compute a larger bottom stress at the next time step than the value which would be computed by 'true' near bottom velocity. When the velocity increases towards the peak current and non-constant stress effects becomes more important, the model with large Δz overestimates the bottom stress. Inclusion of the correction terms in the 10 layer model completely eliminate the error introduced by the model using a larger Δz.
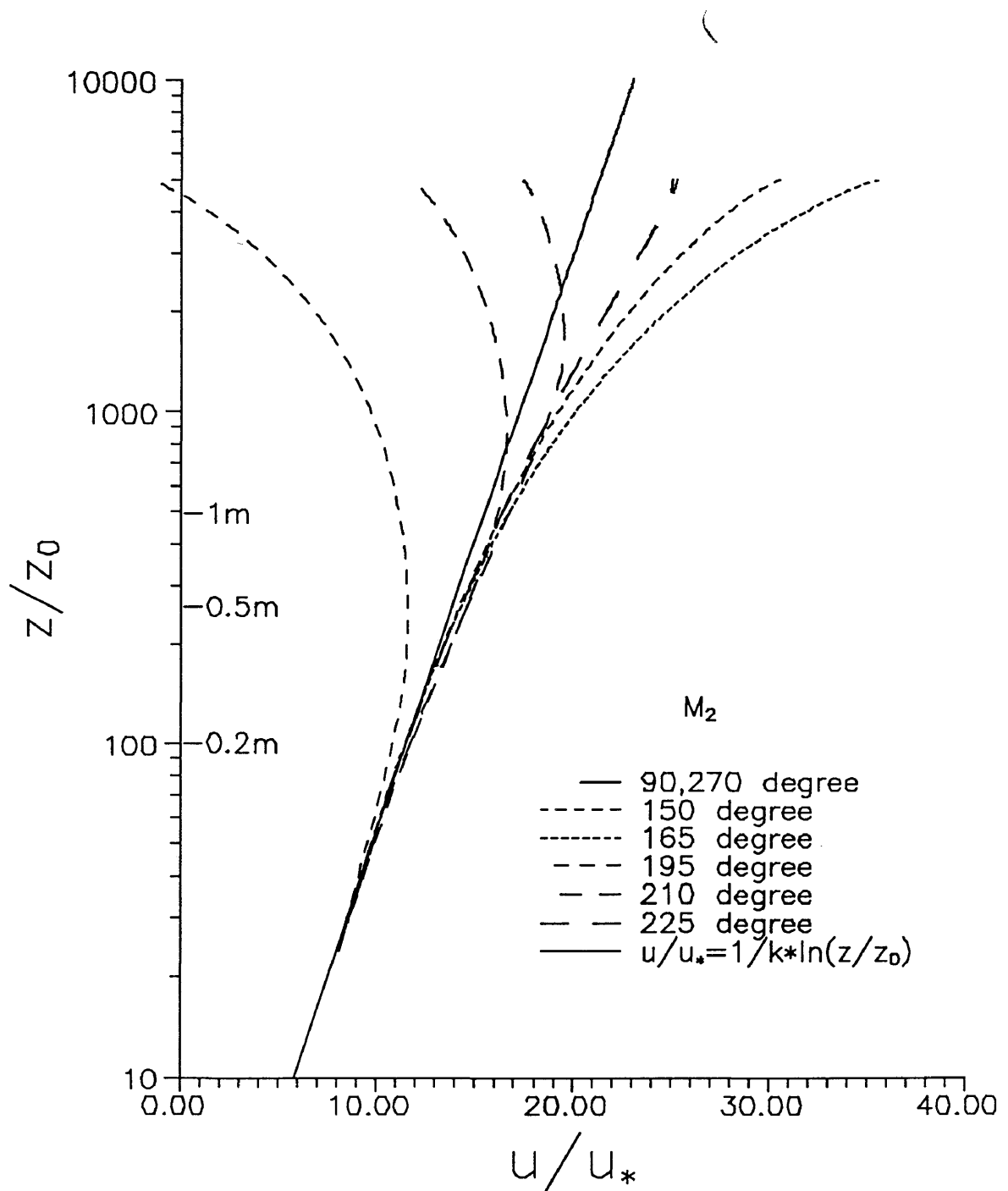
Figure 7. Comparison of vertical velocity distributions with a logarithmic profile (M_2 tide, 90 degree is maximum flood).
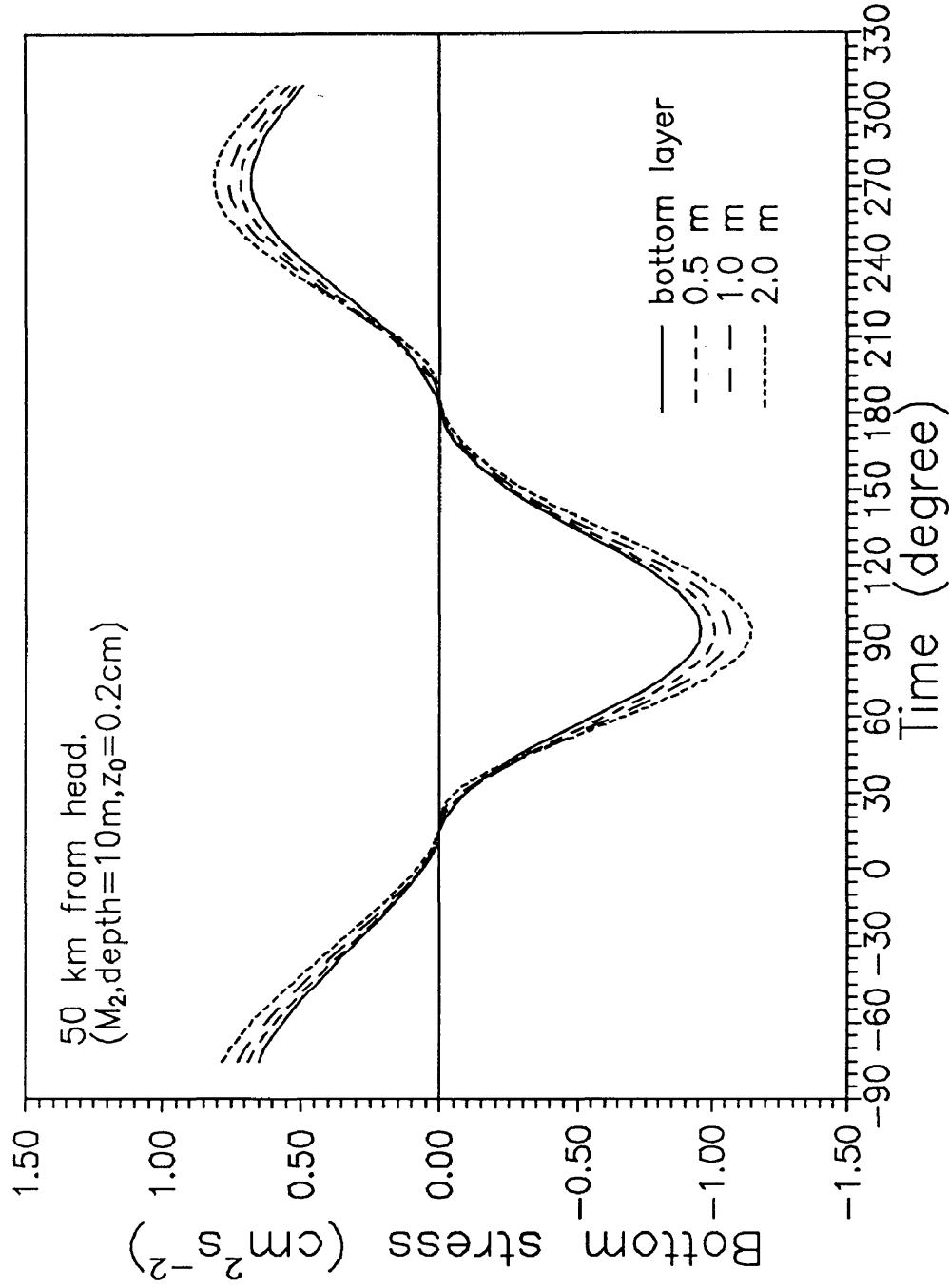
Figure 8. Bottom stress calculated from the velocity at a given height above the bottom assuming a logarithmic velocity profile and known roughness height (M_2 tide).
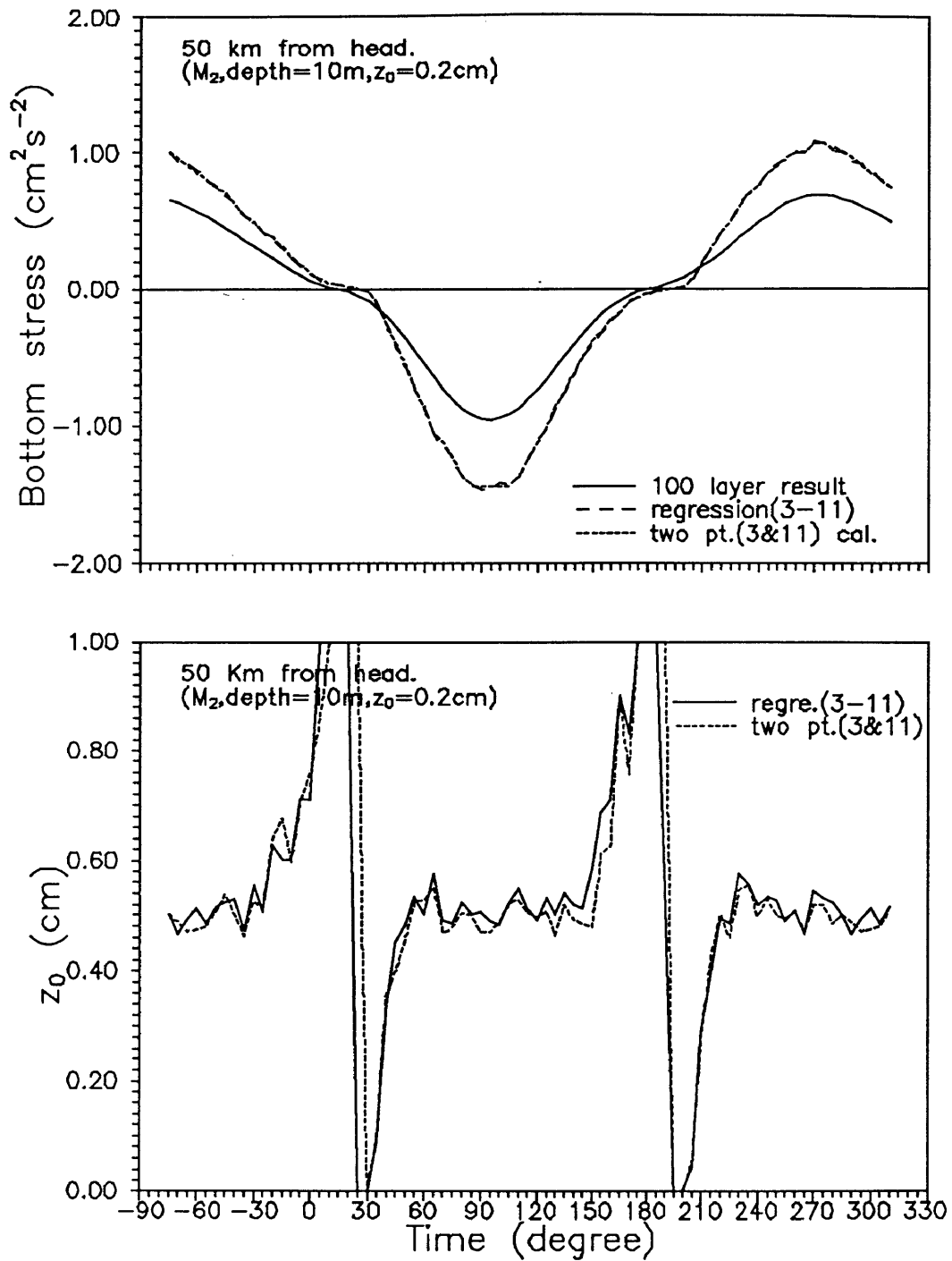
Figure 9. Bottom stress and roughness height calculated by fitting the velocities at more than one height with a logarithmic profile, (a). bottom stress, (b). roughness height.

50.0 km from head.
(M_2,depth=10m,z_0=0.2cm)

bottom layer
0.5 m
1.0 m
2.0 m

Bottom stress ($cm^2 s^{-2}$)

Time (degree)

−90 −60 −30 0 30 60 90 120 150 180 210 240 270 300 330

1.50 1.00 0.50 0.00 −0.50 −1.00 −1.50
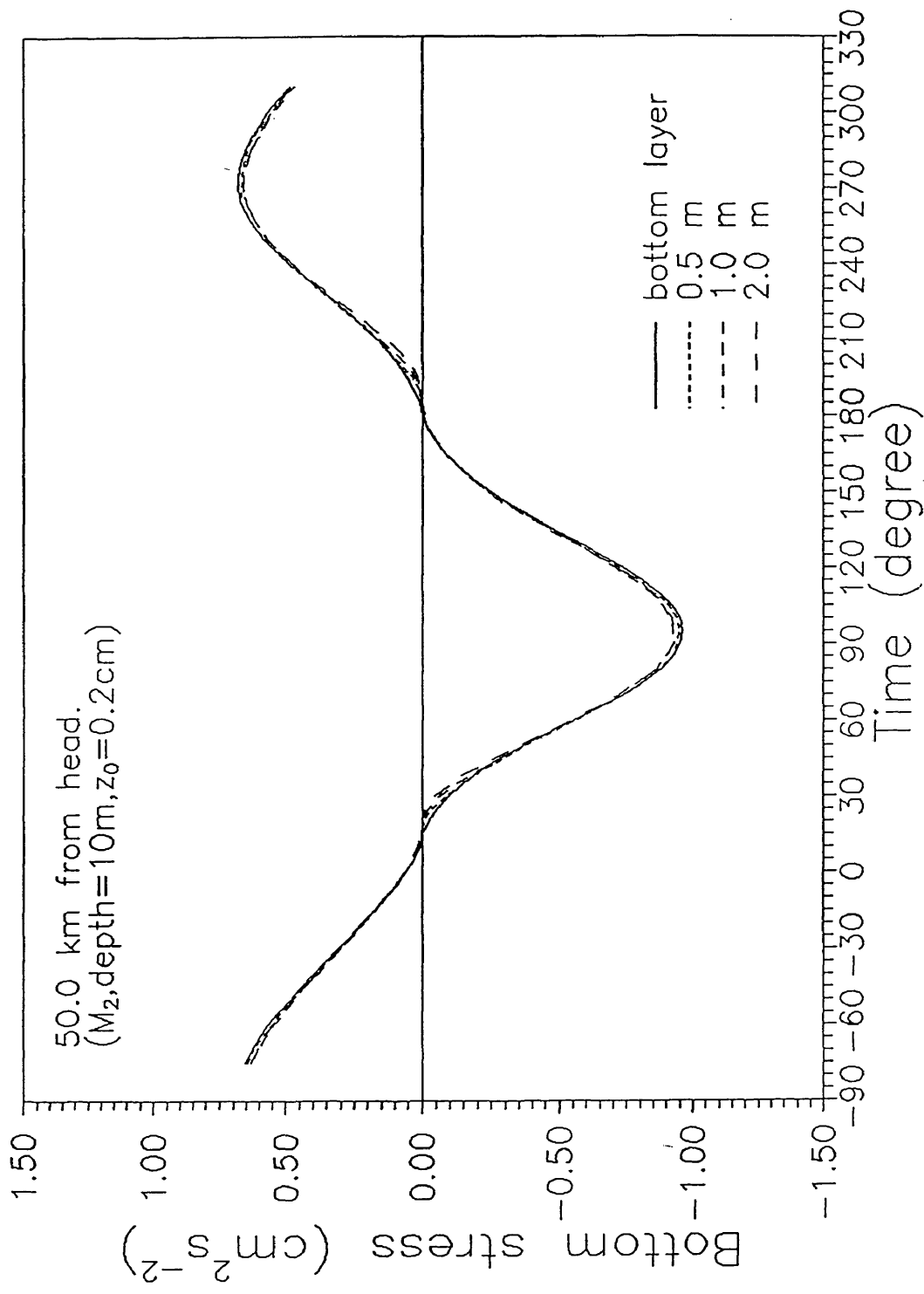
Figure 10. Bottom stress calculated from the velocity at a given height above the bottom assuming a log-linear velocity profile and known roughness height (M_2 tide).
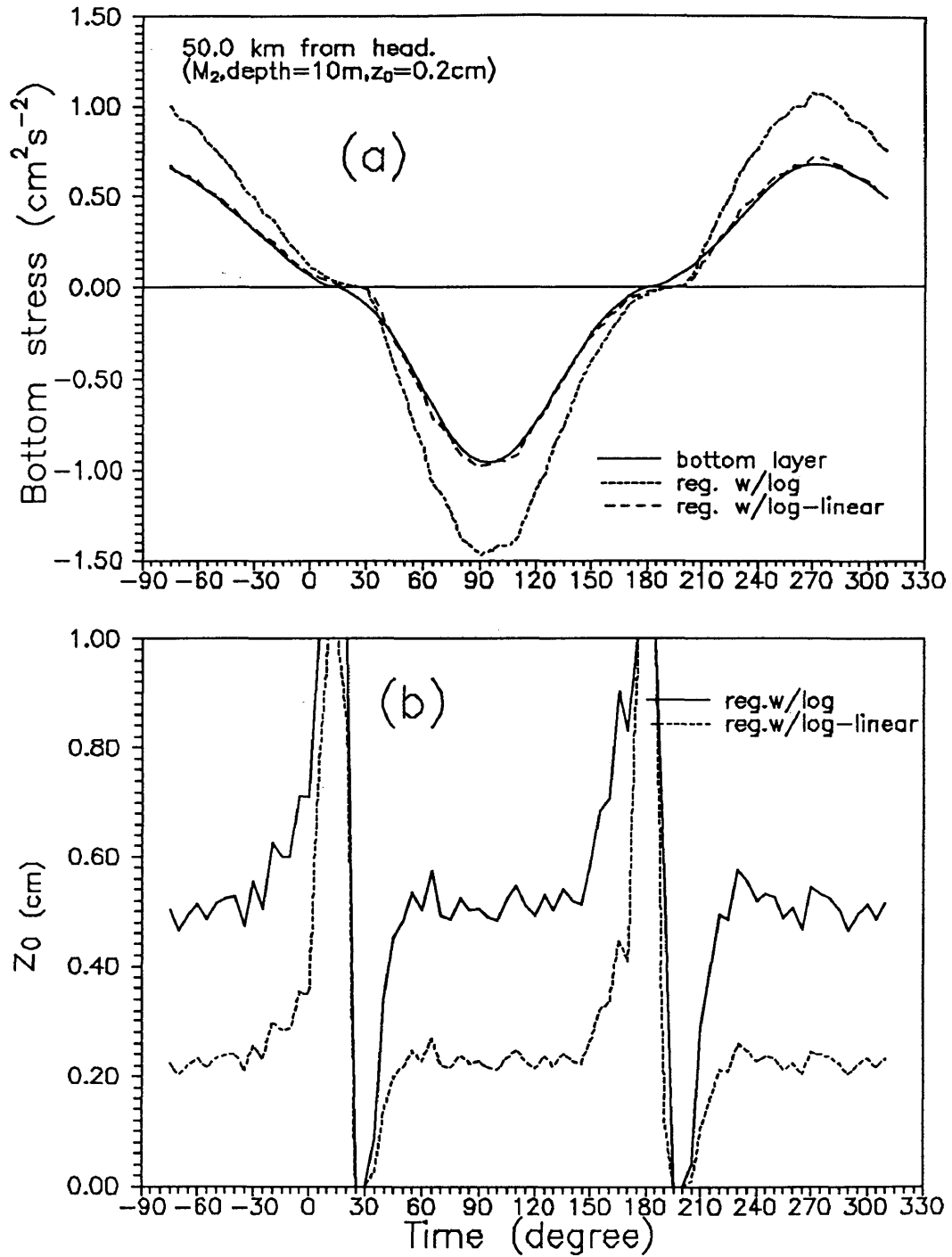
Figure 11. Bottom stress and roughness height calculated by fitting the velocities at more than two heights with a log-linear profile (equation 2.2.5), (a). bottom stress, (b). roughness height.
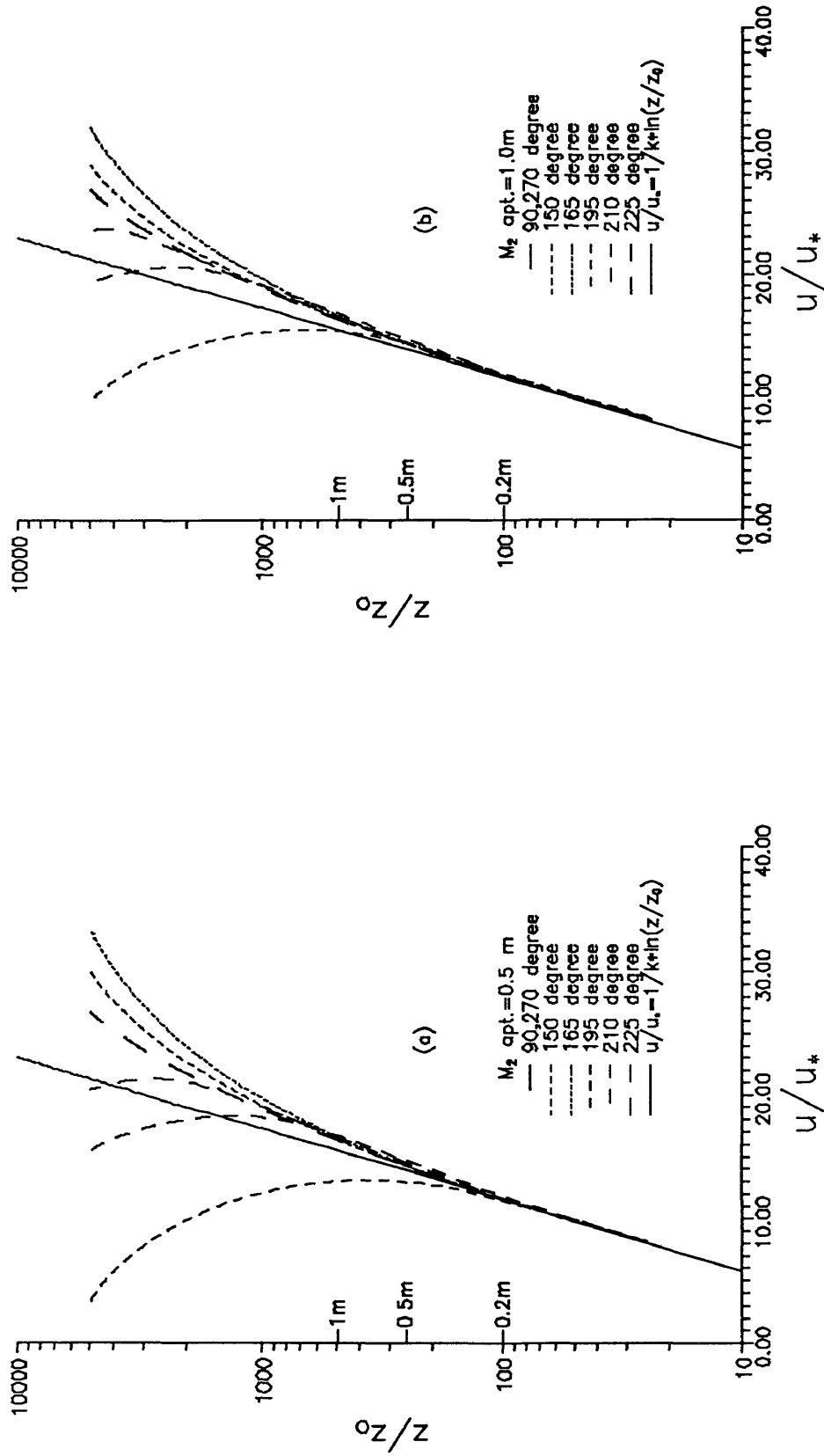
Figure 12. Comparison of vertical velocity distribution with a logarithmic profile, (a) tidal amplitude=0.5m and (b) tidal amplitude=1.0m. (M_2 tide, 90 degree is maximum flood).
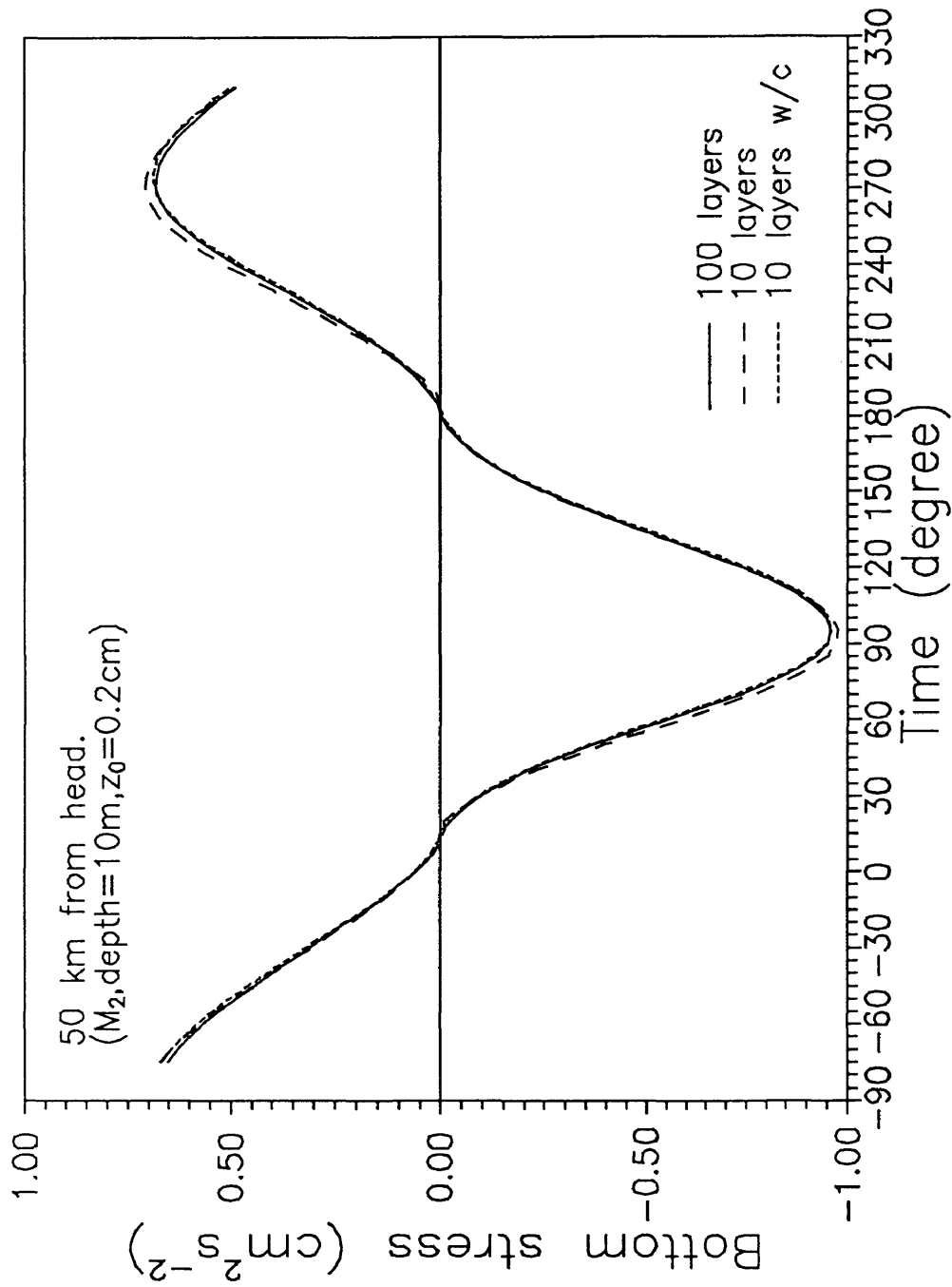
Figure 13. Comparison of bottom stress calculated by the 100 layer model and 10 layer models with and without the corrections (M_2 tide).

4.4 Experiments with an M_8 Tide

To amplify the effect of flow acceleration, the hypothetical estuary was forced with an M_8 tide of 0.25m amplitude. The model was run with 100 layers with and without the first order correction terms. Again, the solutions for the two cases are essentially the same. Figure 14 presents the vertical velocity profiles for various phases of the tide. It shows that the velocity profile deviates from a logarithmic velocity profile above z=50cm for all phases of tide. At the early stage of flow acceleration after slack tide (phase of 195°), the velocity distribution does not follow the logarithmic profile at all. Therefore if bottom stress is calculated using a measured velocity at z>50cm with equations (1.1.3) and (1.1.4) or using regression method, a significant deviation from the 'true value' (i.e., the bottom stress calculated from velocity at z=5cm, with or without the correction terms) will occur. Figures 15 present the bottom shear stress calculated from the velocity at various heights assuming a logarithmic velocity profile. It shows that the bottom stress is underestimated during acceleration and overestimated during deceleration when inertia is dominate. When the effect of non-constant stress becomes dominant, the bottom shear stress is overestimated.

The model was then run with 10 layers with and without the correction terms. The 'with correction' case uses equation (3.3.5). The resulting bottom stress is compared with that predicated by the 100 layer model in figure 16. The results show that the incorporation of the correction terms can almost eliminate the difference between the models using different Δz's. The relative error in calculated bottom stress between the 100 layer and the 10 layer models are presented in Figure 17. The figure shows that the difference relative to the instantaneous bottom stress can reach as high

as 20% if the correction terms are not implemented in the model.

The temporal variations of tidal currents in estuaries are not always symmetrical. Current distortion often occurs at certain locations in estuaries. Therefore, the effect of acceleration will depend on the shape of the tide and its impact on the bottom stress will vary at different locations in the estuary. Figure 18 presents the bottom stresses calculated from 100 layer model and 10 layer model with and without the corrections at another two locations in the estuary. One is near the nodal point (26.25km) and the other is near the mouth (37.25km). Figure 19 shows the relative errors in calculated bottom stress between the 100 layer and the 10 layer models. It can be seen that the effects of acceleration on the bottom shear stresses varies with locations. Comparing three locations in the estuary, the acceleration effect is most pronounced near the head of estuary. Again, incorporating of the correction terms in the model can almost eliminate acceleration effects due to using large Δz's.

Because the frequency of M_8 tide is four times as high as that of M_2 tide, the acceleration effect of M_8 tide is more significant than that of M_2 tide. The logarithmic layer is more depressed. In this case, using regression method to calculate the bottom shear stress, a significant error may occur if data used in calculation are far away from the bottom. The error introduced into the calculation is not only because of the acceleration effect, but also because of effect of non-constant shear stress. Again, we calculate bottom stress and roughness height by fitting the calculated velocities with a logarithmic profile. The velocity data between z=15cm and z=105cm (total of 9 data points) were used in regression. Results presented in figure 20(a) and 20(b) show that significant errors not only occur around slack tide, but also occur around the peak. This indicates that bottom stress calculated in this fashion will result in an overestimate of stress as high as two times, even when there is no significant flow

acceleration. The same procedure used for the M_2 tide experiment was used to fit data with the log-linear profile (equation 2.2.5). The model results were obtained, taking the amplitude of the bottom stress $u_*=1.1$cm, $\sigma=5.6\times10^{-4}$rad s^{-1}, and $u_s=0.2$m, we get $\delta_c=0.44$m and $z_p=1.2$m. The regression results for bottom stress and roughness height are also presented in figures 20(a) and 20(b), respectively, which shows much improvement. Again, the results around the slack tide are still not satisfactory. This indicates that the correction for the acceleration effect is necessary when acceleration is significant.

The calculated velocities near the bottom are presented in Figure 21. The bottom layer velocity for the model with 10 layers is at z=50cm. For the model with 100 layers, the velocities of the 5th (z=45cm), and average velocity of the 5th and 6th (z=55cm) layers are presented. The figure shows that correction terms have much less effect on velocity than bottom stress.
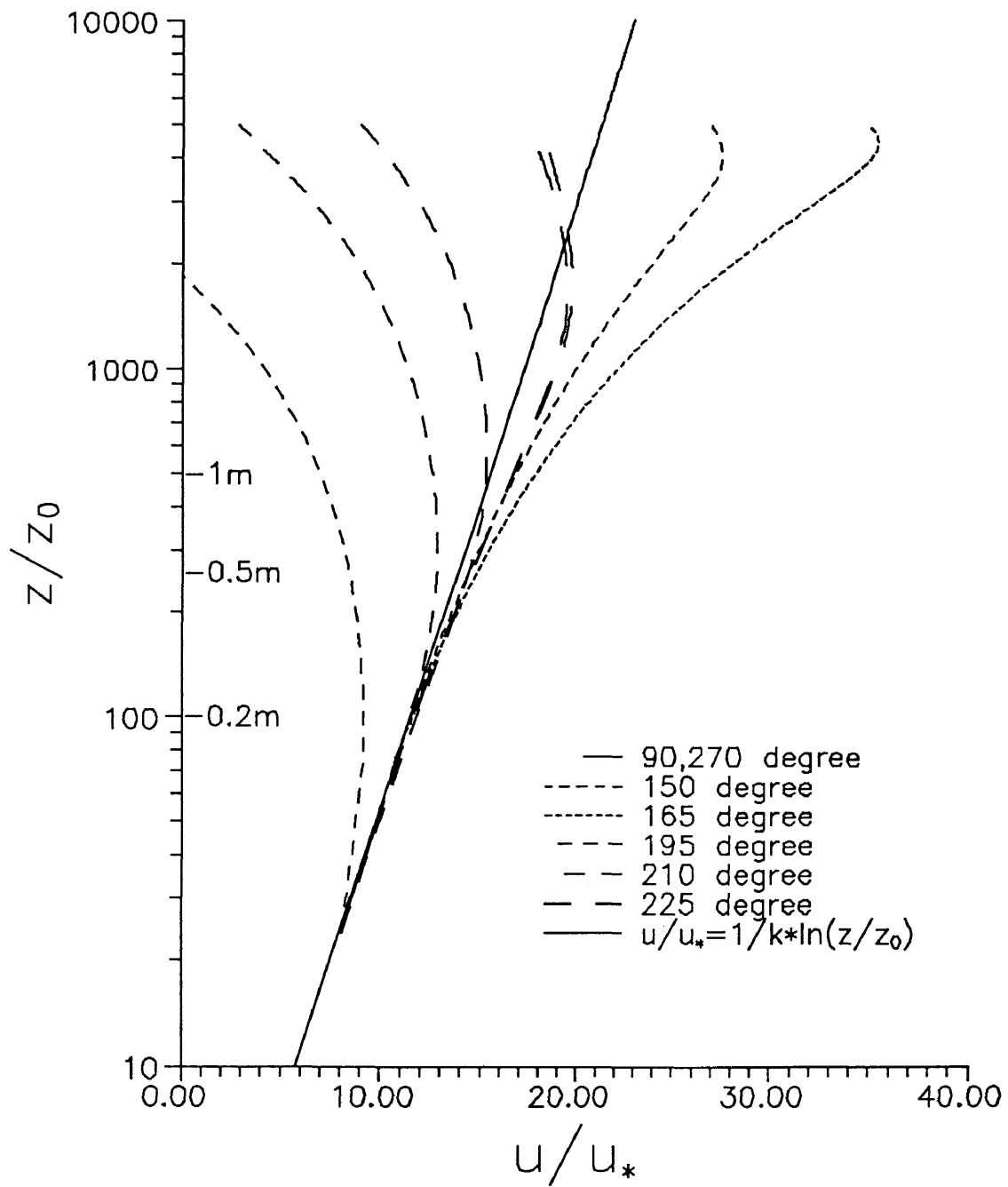
Figure 14. Comparison of vertical velocity distribution with a
logarithmic profile (M_8 tide, 90 degree is maximum flood).
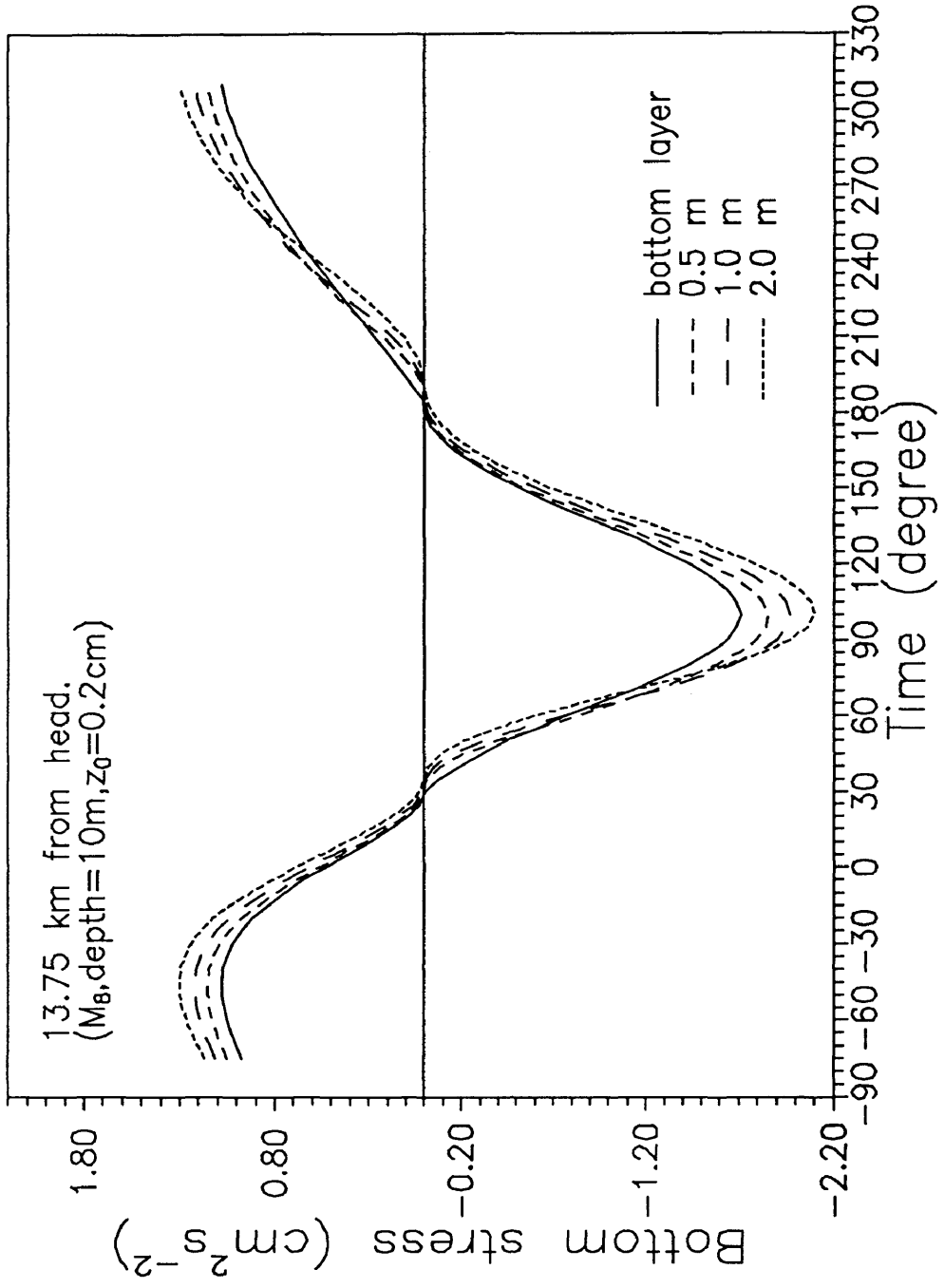
Figure 15. Bottom stress calculated from the velocity at a given height above the bottom assuming a logarithmic velocity profile and known roughness height (M_8 tide).
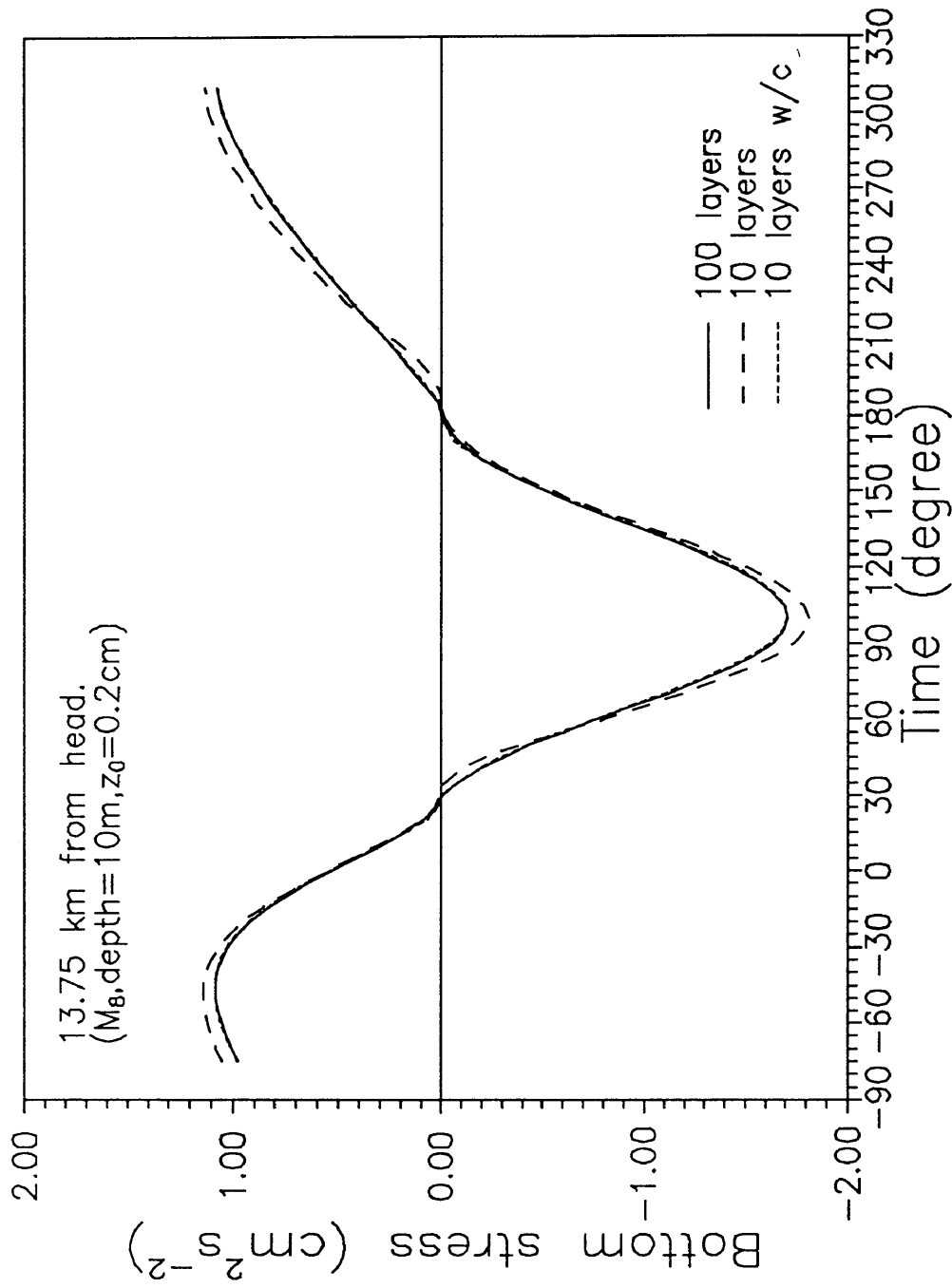
Figure 16. Comparison of bottom stress calculated by the 100 layer model and 10 layer models with and without the corrections (M_8 tide 13.8 km from the head).
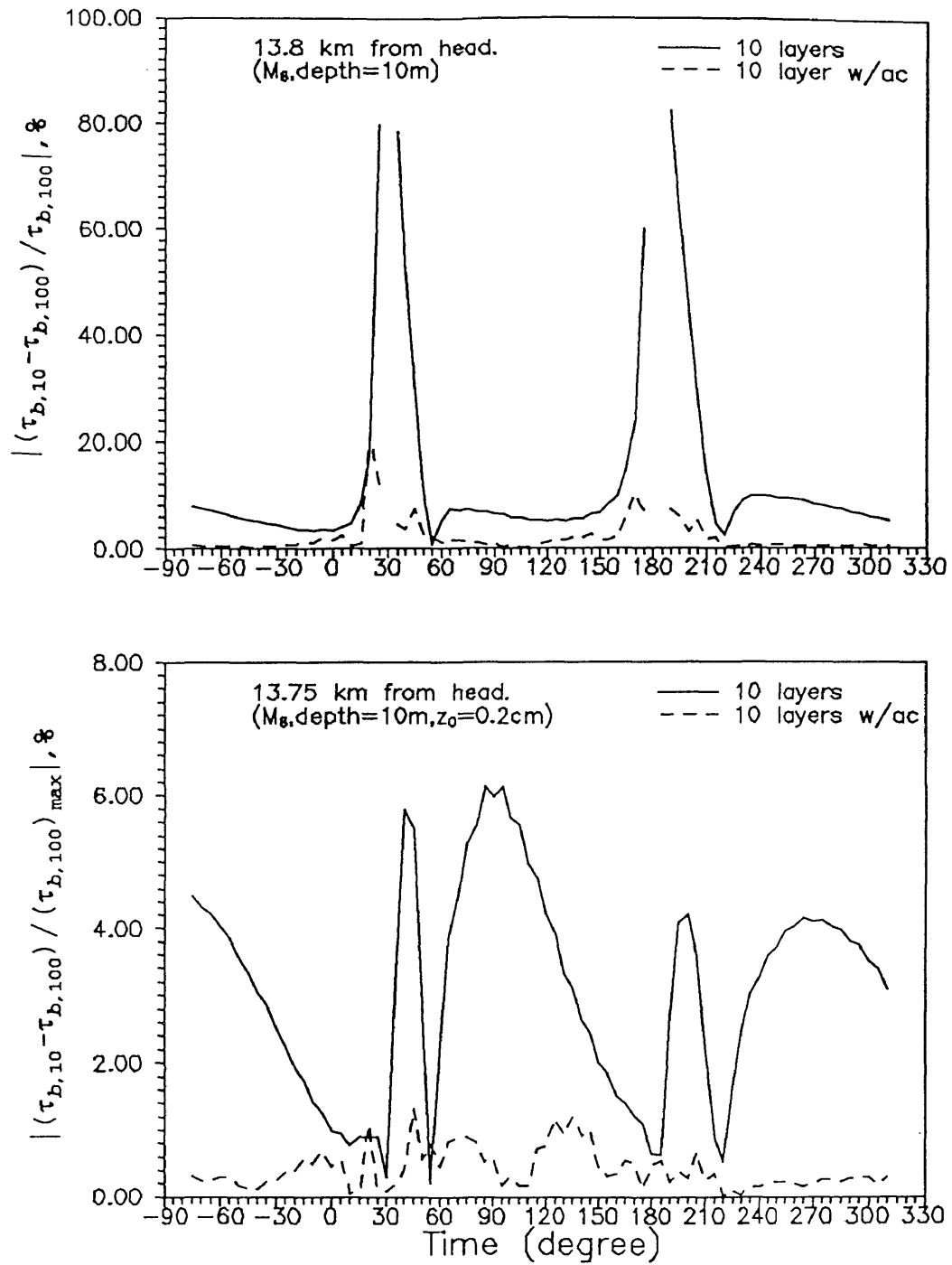
Figure 17. Relative error of bottom stress calculated by 10 layer models (M_8 tide), (a) relative to instantaneous bottom stress, (b). relative to the maximum bottom stress.

(a) chart

26.25km from head.
$(M_8, \text{depth}=10m, z_0=.2cm)$

(a)

4.00

2.00

0.00

-2.00

-4.00

Bottom stress $(cm^2 s^{-2})$

Time (degree)
-90 -60 -30 0 30 60 90 120 150 180 210 240 270 300 330

——— 100 layers
- - - 10 layers
- - - - 10 layers w/c

(b) chart

38.75 km from head.
$(M_8, \text{depth}=10m, z_0=.2cm)$

(b)

4.00

2.00

0.00

-2.00

-4.00

Bottom stress $(cm^2 s^{-2})$

Time (degree)
-90 -60 -30 0 30 60 90 120 150 180 210 240 270 300 330

——— 100 layers
- - - 10 layers
- - - - 10 layers w/c
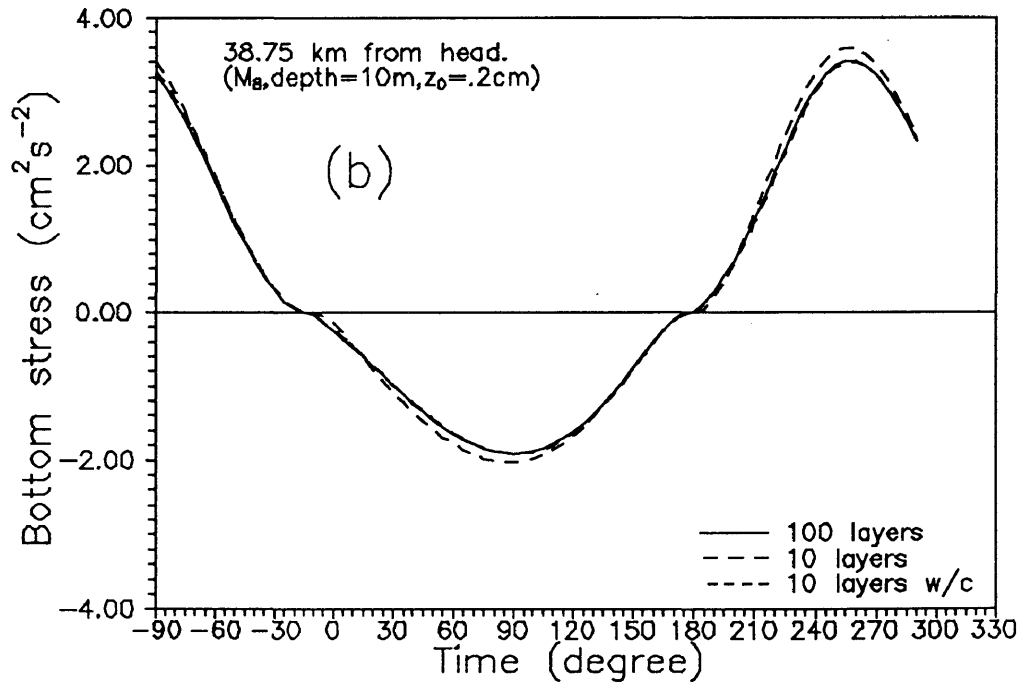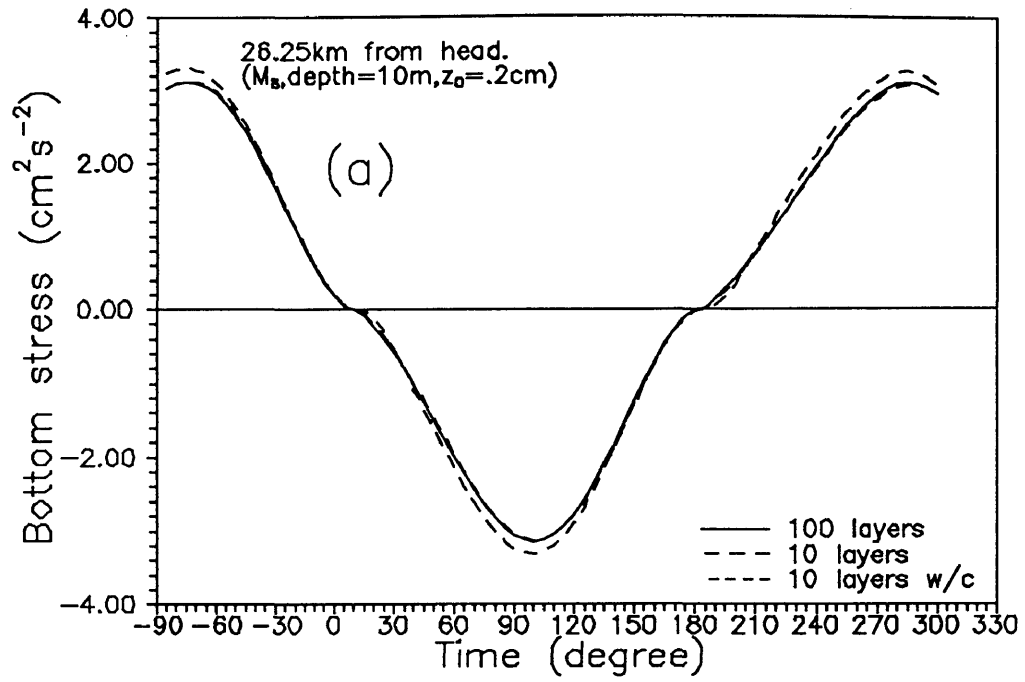
Figure 18. Comparison of bottom stress calculated by the 100 layer model and 10 layer models with and without the corrections (M_8 tide). (a) 26.25km from the head. (b) 38.75km from the head.
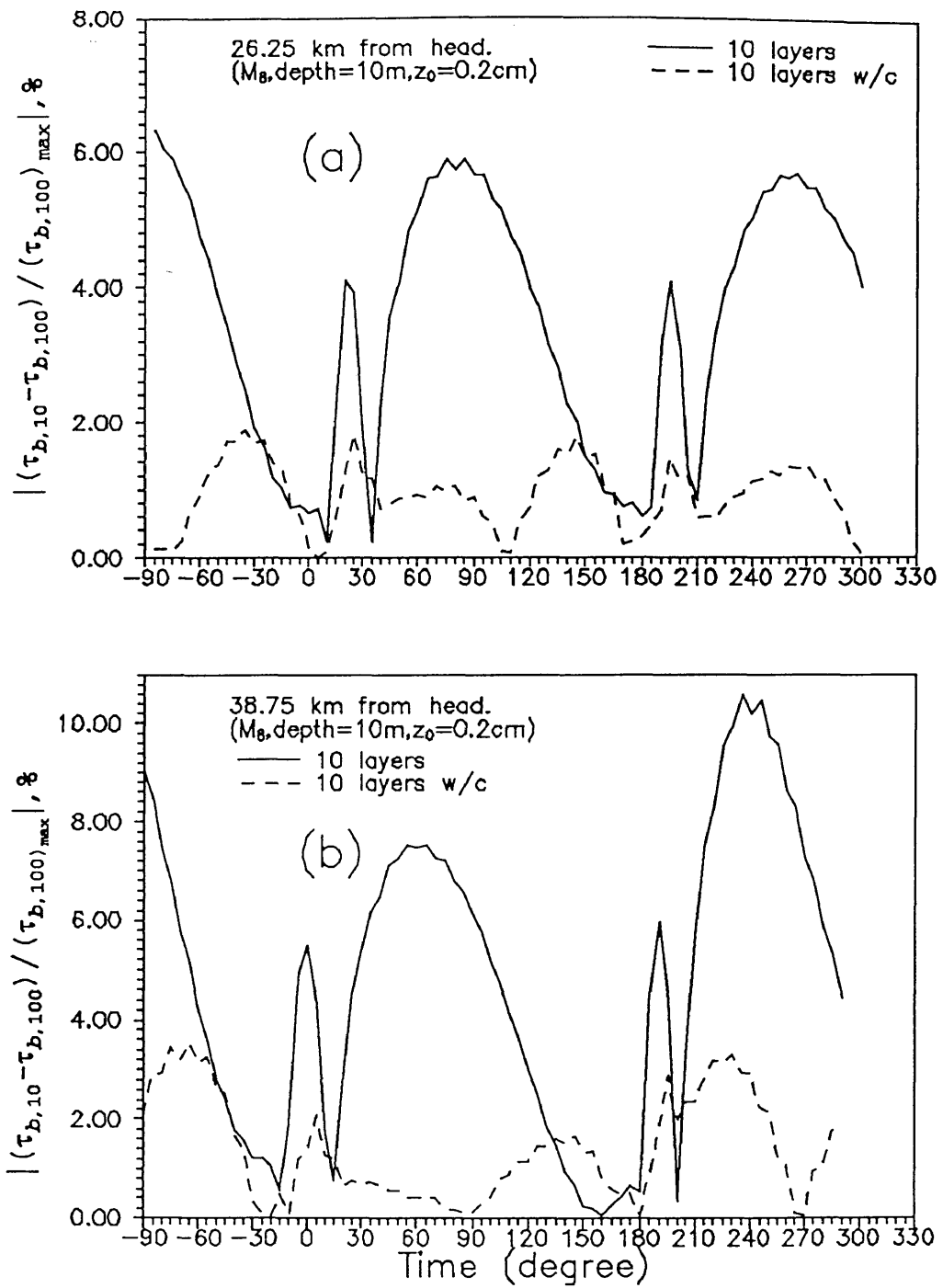
Figure 19. Relative error of bottom stress calculated by 10 layer models, relative to maximum stress (M_8 tide). (a) 26.25km from the head. (b) 38.75km from the head.
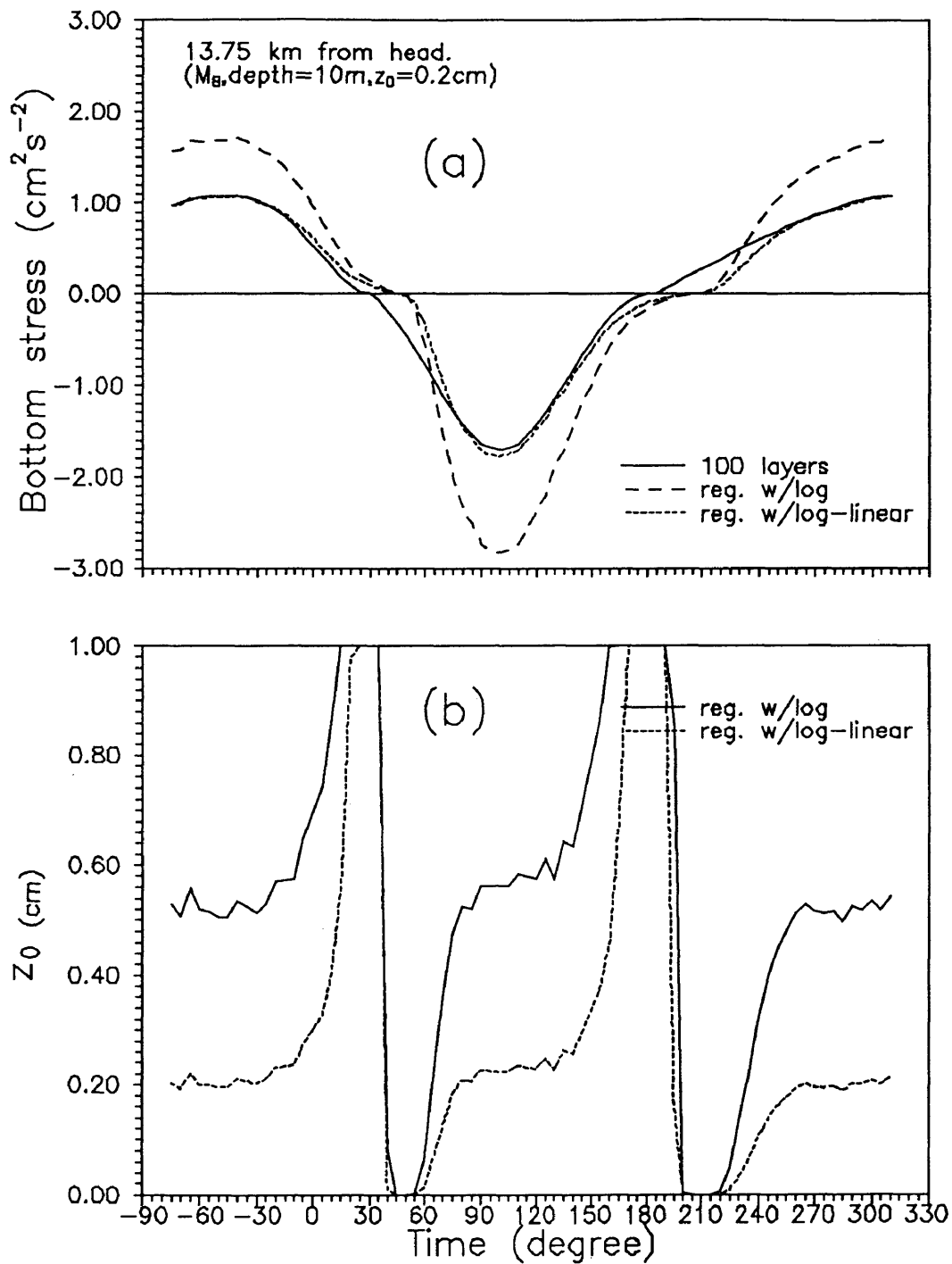
Figure 20. Bottom stress and roughness height calculated by fitting the velocities at more than two heights with a logarithmic profile and with a log-linear profile (M_8 tide). (a) bottom stress, and (b) roughness height.
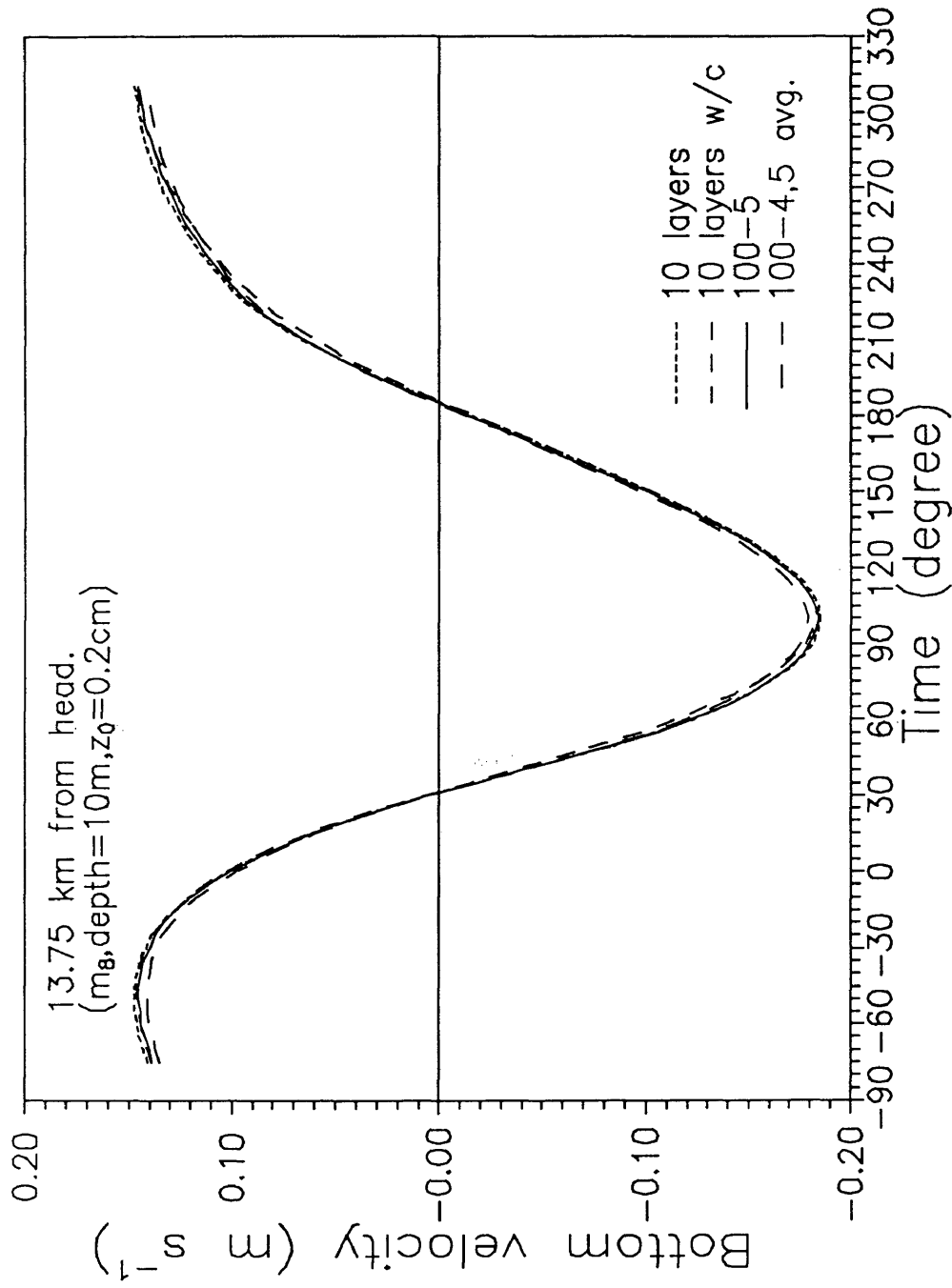
Figure 21. Comparison of the calculated velocities at the bottom layer of the 10 layer models with those of the 100 Layer model at roughly correspondent heights.

5 SUMMARY AND CONCLUSIONS

5.1 Introduction

Using numerical models to simulate the structure of estuarine flows and to calculate sediment transport, one of the fundamental problems is to correctly calculate bottom shear stress which is one of the bottom boundary conditions of numerical model. It is a common practice to calculate bottom stress with a logarithmic velocity profile near the bottom. Because of the unsteadiness of the tidal flow, the inertial effect and the non-constant stress distribution in the water column would result in velocity distribution deviating from the logarithmic profile. An error will be introduced when the magnitude of flow acceleration is large or the grid spacing used in the model is not fine enough. It is particularly important to calculate the bottom stress accurately in a numerical model of sediment transport since the bottom stress dominates the deposition and resuspension processes. Field and theoretical studies summarized in the chapter 1 and 2 indicate that large deviation of velocity from the logarithmic profile may occur and the calculated bottom stress may be in error by as much as 60% if logarithmic velocity profiles is assumed. No simple formula incorporating both inertial and non-constant stress effects is available for use in numerical models. Soulsby and Dyer (1981) suggested a log linear velocity profile which included a correction for acceleration effects. However, their formula can be used only in a constant stress layer. Since the shear velocity is implicitly involved in their equation and the parameter introduced in the equation needs to be pre-determined, it is still difficult for

71

application. The purpose of this study was to derive a simple formula including the correction of inertial and non-constant stress effects to calculate bottom stress in a numerical model. The emphasis of this study was placed on quantifying the effects of flow acceleration and non-constant stress on the bottom stress calculation.

5.2 Summary of the Present Study

The following sections summarize the theoretical and numerical model techniques used in this study to investigate the boundary layer structure in homogeneous tidal flows. The last section summarizes the contributions and the limitations of the present study.

5.2.1 Theoretical study

A long channel having a wide rectangular cross section with a hydraulic roughness height z_0, as illustrated in Fig.2, was selected for theoretical analysis. To isolate the essential mechanisms, only homogeneous unsteady flow is considered in the present study. The simplified boundary layer equation is given by equation (2.1.1). The analysis assuming constant stress layer is given in section 2.1 and the effect of non-constant stress is discussed in section 2.2.

The boundary layer equation is written in a dimensionless, finite difference form by introducing the velocity deficit $u_d = u - \bar{u}$ to cast it into a form suitable for perturbation analysis. The complete set of equations and boundary conditions for the perturbation solution are given in section 2.1 (equations 2.17 to 2.19, and 2.11 to

2.13). The solution for the velocity profile, assuming constant stress layer, is given by equations (2.1.20) or (2.1.28). The solution for the velocity profile consists of two parts, the logarithmic profile and the linear correction term for inertial effects. Equation (2.1.28) has the same form as that presented by Soulsby and Dyer (1981) while no unknown parameter is introduced. The bottom stress was obtained by solving the velocity profile equation (2.1.20) and the result is given by equation (2.1.25). Based on these results, the error of neglecting acceleration effect is further quantified. The relative error of calculated bottom share stress, if acceleration effect is neglected, is given by equation (2.1.33). The error of omitting acceleration not only depends on the magnitude of the flow acceleration but also depends on the distance from the bottom where velocity is used for the bottom stress calculation. The error between the true stress and bottom roughness and those estimated by regression techniques can be estimated by equations (2.1.36a) and (2.1.40), respectively.

In section 2.2, the effect of non-constant stress near the bottom was considered. By introducing a new formulation for eddy viscosity, the zero order boundary layer equation was solved to obtain the velocity profile (equation 2.2.5), in which the assumption of constant stress layer is removed. Using equation (2.2.5) to calculate bottom stress, knowledge of z_p, a new parameter introduced in the formula, is required. However, it can be estimated by an empirical equation (2.2.14) together with equation (2.2.1a) or using equation (2.2.19) in a numerical model. By combining the effect of flow acceleration and the non-constant stress effect, the formulation of bottom stress calculation in a numerical model is given by equations (3.3.3). The method of specifying the bottom boundary layer condition in the numerical model is summarized in section 3.3.

5.2.2 The Numerical Model Study

The numerical experiments were conducted in a hypothetical estuary (figure 2) with a single M_2 or M_8 tide of 0.25m amplitude forcing at the mouth. A constant roughness height of $z_0=0.2$cm was used throughout the experiments. Chapter 4 describes all the model experiments. The results of M_2 tide experiments are presented in section 4.2 and the results of M_8 tide experiments are presented in section 4.3.

The experiments were designed first to verify one of the conclusion of the theoretical study: as long as a very close to the bottom velocity is used to calculate the bottom stress, no significant error will be introduced in a model even if the logarithmic profile is used for bottom stress calculation. The model experiments were conducted by running the model with 100 layer vertical resolution and specifying the bottom stress 'with' and 'without' correction, respectively. The 'without' case assumes a logarithmic velocity profile and uses equation (1.1.5) to specify boundary condition. The 'with correction' case uses equation (3.3.5) to calculate bottom stress. The results of two experiments gave essentially the same results which is expected from the theoretical analysis. Experiments were further conducted to examine the error introduced in the bottom stress calculation 'with' and 'without' corrections. The error in calculating the bottom stress with a logarithmic velocity profile was determined by using velocity output from a 100 layer model at different layers. Two methods of calculating bottom stress were tested; one used velocity at a single height and known roughness height, and the other used regression to fit the velocity data with a logarithmic profile to estimate the bottom stress and roughness height. If the 'without correction' equations were used, both methods gave unsatisfactory results. The errors between calculated values and the model results are presented in Figures 8 and 9, respectively. The results of using equations 'with correction' are presented in figures

10 and 11, respectively. It shows that results of using equations 'with correction' are very satisfactory. The applicability of the formulation obtained from this study in the numerical model was tested by running model with lower vertical resolution (10 layers). Runs specifying the bottom stress boundary condition 'with' and 'without' corrections were compared with the results of 100 layer model. The error for M_2 and M_8 tides with large grid spacing are presented in figure 13 and 16, respectively.

5.2.3 The contribution and Limitation of the Present Study

The present study successfully derived a formulation for bottom stress which incorporates both inertial and non-constant stress effects into a simple equation. The new equation relates the bottom stress to the velocity and acceleration computed in the bottom layer of a numerical model so that the equation can adequately be used to specify the bottom boundary condition. For a practical range of vertical grid spacing in numerical models of estuarine flows, the inclusion of correction terms can significantly reduce the error introduced by finite grid spacing. The equation can be applied to a numerical model in estuary. The equation can also be used to quantify the error introduced if acceleration and non-constant stress effects are not accounted for. The near bottom velocity profile obtained from the present study shows the vertical flow structure in homogeneous tidal flow and identifies situations when the flow acceleration and non-constant stress effects are important. Because it is derived in a finite difference form, the formula presented in this study is more suitable for a numerical model rather than in situ application. When used in a numerical model, a relative large Δt may be required to elaborate ξ. Some problems may arise if a small Δt must be used. In that case, tidal mean eddy viscosity may be used to re-scale the boundary layer equation to get an overall acceleration correction so that the

discontinuity at zero shear velocity can be avoided. For field applications to estimate roughness and shear stress by regression method, knowledge of the parameter z_p is needed. Although equations (2.2.1a) and (2.2.14) give an estimation of z_p, their use in the field is limited.

5.4 Conclusion and Recommendation

In a tidal estuary, the vertical velocity distribution near the bottom may deviate from a logarithmic profile because of three reasons: first, the flow unsteadiness suppresses the thickness of the constant stress layer, thus reducing the domain in which logarithmic profile may be applicable; second, the inertia effect of flow acceleration and deceleration makes the velocity deviate from the logarithmic profile even within the constant stress layer; and third, the flow stratification may be strong enough that the buoyancy effect is not negligible. Away from the bottom, the flow is affected by external conditions. Because of the phase lead near the bottom, the reversals of the bottom flow and the flow away from the bottom do not occur simultaneously. The flow away from the bottom responses to flow acceleration slower than bottom flow. Thus, the inertia effect increases with the distance from the bottom. For a given roughness height, the error in the bottom stress calculated from a logarithmic velocity profile increases with the distance at which the velocity is used for stress calculation. Since the flow acceleration is most significant around slack tide, the first order correction for the inertia effect is more important around slack tide when the bottom velocity is small. The bottom stress calculated from the logarithmic profile is underestimated during flow acceleration and overestimated during flow deceleration. If the bottom roughness height is estimated by fitting data to the logarithmic profile, it will also be overestimated during flow deceleration and

underestimated during flow acceleration, in particular, around the slack water. The error introduced for roughness height calculations is more significant than that for bottom stress calculation. The error of calculated bottom stress and roughness height increases with tidal frequency and becomes significant when overtides are present. However, the time duration when inertia effects are important is relatively short compared to the tidal period.

Normally shear stress increases form zero at surface with depth. For a given total depth, the larger the bottom stress, the larger its vertical gradient is, and the difference in shear stress at different levels will be more significant even near the bottom. In other words, the constant stress layer is suppressed when the bottom stress is large. Because large bottom stresses corresponds to the large bottom velocities, the effect of the constant stress layer suppression increases with flow velocity. Significant errors may occur if a logarithmic velocity profile is used to estimate bottom stress and roughness height when the velocity data used are outside of the constant stress layer. The effect of non-constant stress will always overestimate bottom stress and bottom roughness height. The error increases with flow velocity and the distance at which the velocity is used for calculation. The calculated values of roughness height and bottom stress may be off by more than 100% in situation where the effect of non-constant stress is significant.

Because of negative feedback in numerical computations, the error resulting from the logarithmic profile assumption in numerical model is reduced. If the vertical grid spacing of a numerical models is fine enough, the use of the logarithmic profile to calculate the bottom stress should result in a negligible error. With practical ranges of vertical grid spacings, the error in bottom stress calculated by the logarithmic profile becomes significant, particularly when overtides are present. The incorporation of the

correction terms derived in this study are able to eliminate the problem of using larger grid spacing. The velocity computed by the model is much less sensitive to the logarithmic profile assumption. There is a slight difference between the first layer velocities calculated, respectively, with and without the correction terms. Beyond the first layer, no noticeable difference between the calculated velocities exists.

Since the flow is highly affected by external conditions in the outer layer, the reversals of bottom stress and velocity well above the bottom do not occur simultaneously for oscillatory flow. Therefore, the friction coefficient will depend on the frequency of oscillation and the roughness height. The correction for the friction coefficient given in this study makes it possible to relate bottom stress to the velocity above the bottom. The numerical experiments show that the formulation of bottom stress calculation is very efficient for use in models. However, the equation derived in this study is more suitable for a numerical model than for in situ bottom stress calculation. For field application, the lowest current measurement is seldom closer than 15cm to the bed. When regression techniques are used to estimate bottom stress and roughness height, the knowledge of z_p is required which functions as the correction of extrapolating measured velocity profile towards the bed. Since this parameter is a function of the thickness of the constant stress layer, it is an unknown parameter before the bottom stress is known. Another difficulty is that z_p is incorporated in the coefficient for linear correction term in the velocity profile and. The linear term is highly correlated with the logarithmic term in the velocity profile and it is not statisticly independent so that regression may not give satisfactory results. More quantitative investigations of the parameter z_p and the model for eddy viscosity in an oscillatory flow are desirable in future studies.

In the prototype estuarine flow, the benthic boundary layer is complicated by

interaction of flow oscillation, sediment movement, and stratification. The salinity and suspended sediment often produce stable stratification within the boundary layer, thus inhibiting turbulence and vertical flux of mass and momentum and resulting in non-logarithmic velocity distributions. The effect of interactions between flow oscillation and stratification on the bottom stress further complicates the problem. Therefore, further theoretical and field investigations of turbulent boundary layer structure in oscillatory stratified estuarine flow are warranted.

LITERATURE CITED

Anwar, H.O., 1981: A study of the turbulent structure in a tidal flow. Estuarine, Coastal and shelf Science. 13, 373-387.

Anwar, H.O., 1983: Turbulence measurements in stratified and well-mixed estuarine flows. Estuarine, Coastal and shelf Science. 17, 243-260.

Arya, S. P. S., 1973: Neutral planetary boundary layer above a nonhomogeneous surface, Geophys. Fluid Dyn., 4, 333-355.

Blumberg, A.F. and G. L. Mellor, 1987: A description of a three-dimensional coastal ocean circulation model. Three-dimension coastal ocean models, Norman S. Heaps, Editor p. 208, American Geophysical Union.

Dyer, K. R., 1986: Coastal and Estuarine Sediment Dynamics, Wiley-In-terscience, New York, 342.

Galperin, B., L. H. Kantha, S. Hassid, and A. Rosati, 1988: A quasi-equilibrium turbulent energy model for geophysical flows. J. Atmos. Sci., 45, 55-62.

Gross, T. F., and A. R. M. Nowell, 1983: Mean flow and turbulence scaling in a tidal boundary layer. Continental Shelf Res., 2 ,109-126.

Hamrick, J. M., 1992: A Three-Dimensional Environmental Fluid Dynamics Computer
    Code: Theoretical and Computational Aspects. Virginia Institute of Marine
    Science, Gloucester Point. Va. Spec. Rep. in App. Mar. Sci. and Ocean Eng.,
    139.

Hinze, J. O., 1975: Turbulence, 2nd edition, McGraw Hill, Anckland.

Jonsson, I. G. and N. A. Carlsen, 1976: Experimental and theoretical investigations in
    an oscillatory turbulent boundaty layer, J. Hydraul. Res., 14, 45-60.

Lavelle, J. W., and H. O. Mofjeld, 1983: Effects of time-varying viscosity on
    oscillatory turbulent channel flow. J. Geophys. Res. 88(C12), 7607 -7616.

Lundgren, H., 1972: Turbulent currents in the presence of wave. paper presented at
    13th Coastal Engineering and Research Conference Am. Soc. Civil Eng., New.
    York, N.Y.

Mellor, G. L., and T. Yamada, 1982: Development of a turbulence closure model for
    geophysical fluid problems. Rev. Geophys. Space Phys., 20, 851-875.

Soulsby, R. L., and K. R. Dyer, 1981: The form of the near-bed velocity profile in a
    tidally accelerating flow. J. Geophys. Res., 86(C9), 8067-8074.

Soulsby, R. L., 1983: The bottom boundary layer of shelf seas, in Physical
    Oceanography of Coastal and Shelf Seas, John, B., Ed., Elsevier, Amsterdam,
    198.

Sternberg, R. W., 1972: Predicting initial motion and bedload transport of sediment particles in the shallow marine environment, in Shelf Sediment Transport: Processes and Pattern, Swift, D. J. P., Duane, D. B., and Pilkey, O. H., Eds., Dowdon, Hutchinson and Ross, Stroudsburg, Penn., 61.

Wilkinson, R. H., 1986: Variation of roughness length of a mobile send bed in a tidal flow. Geo-Marine Letters, 5, 231-239.

Wright, L. D., 1989: Benthic boundary layers of estuarine and coastal environments. Reviews in Aquatic Sciences. 1, 75-95.

VITA

JIAN SHEN

Born in Shanghai, People's Republic of China, 14 October 1958. Earned B.S.
in Mathematics from Shanghai Teacher's University in 1982. Was a teacher assistant
and a lecturer of Institute of Estuarine and Coastal Research, East China Normal
University for eight years. One year visiting scientist at Netherlands Institute for Sea
Research, Netherlands. Entered master program in College of William and Mary.
School of Marine Science in 1990.